CHALMERS
UNIVERSITY OF TECHNOLOGY

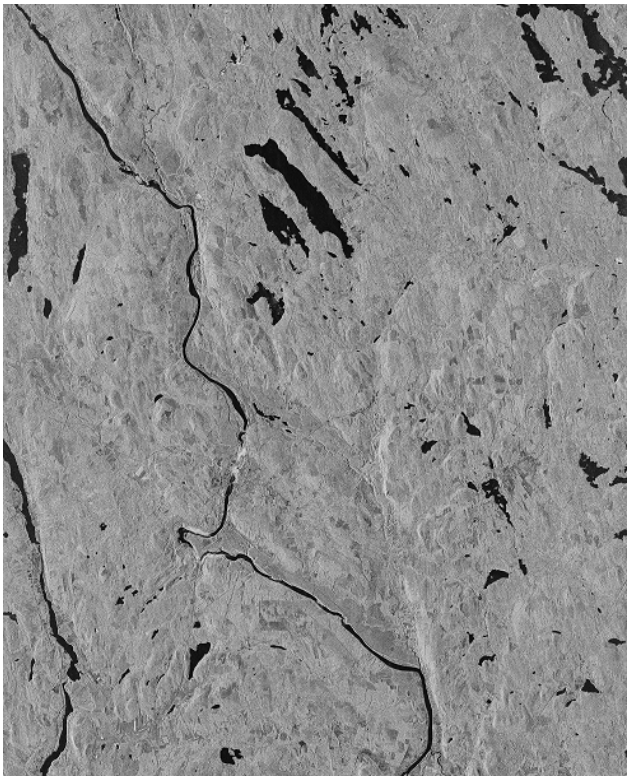

Information Extraction from Spaceborne SAR Data of up to 64-Image Depth Image Stacks.

Investigating statistical models to describe the temporal variations of X-band SAR intensity data.

Master's thesis in Communication Engineering

Adam Hessing

Department of Space, Earth and Environment
CHALMERS UNIVERSITY OF TECHNOLOGY
Gothenburg, Sweden 2020

Master's thesis 2020

Information Extraction from Spaceborne SAR Data of up to 64-Image Depth Image Stacks.

Investigating statistical models to describe the temporal variations of X-band SAR intensity data.

Adam Hessing

CHALMERS
UNIVERSITY OF TECHNOLOGY

Department of Space, Earth and Environment
Chalmers University of Technology
Gothenburg, Sweden 2020

Information Extraction from Spaceborne SAR Data of up to 64-Image Depth Image Stacks.
Investigating statistical models to describe the temporal variations of X-band SAR intensity data.
ADAM HESSING

Supervisor: Gary Smith-Jonforsen, Saab AB
Supervisor: Patrik Dammert, Saab AB
Examiner: Lars Ulander, Department of Space, Earth and Environment, Chalmers

Master's Thesis 2020
Department of Space, Earth and Environment
Chalmers University of Technology
SE-412 96 Gothenburg
Telephone +46 31 772 1000

Cover: SAR intensity data image of Krycklan area in northern Sweden.

Typeset in LaTeX
Printed by Chalmers Reproservice
Gothenburg, Sweden 2020

Information Extraction from Spaceborne SAR Data of up to 64-Image Depth Image Stacks.
Investigating statistical models to describe the temporal variations of X-band SAR intensity data.
ADAM HESSING
Department of Space, Earth and Environment
Chalmers University of Technology

Abstract

The spatial statistics of synthetic aperture radar (SAR) images of the Earth's surface have been extensively studied in the past. Recent commercial projects from several companies will provide a lot of high quality and importantly high quantity of SAR satellite data, which enables the analysis of the SAR images in time (temporal) instead. This thesis has investigated two different image stacks, containing 28 and 64 images respectively, of SAR intensity data. The investigation has focused on how the statistical distributions in time can be characterized. The temporal SAR data have been tested against eight different target distribution models with the Anderson-Darling goodness-of-fit test. The use of the Anderson-Darling test together with looking for spatial patterns have allowed for comparison of how well the target distribution models fit, even with a limited number of images available.
Both statistical and visual interpretations of the results have been made through tables and false-colored images. The results have shown that the distribution of temporal SAR intensity data follows a Gamma distribution irrespective of surface area type. Furthermore, none of the target distributions performed specifically well on areas containing buildings and structures. There was a difference how well the Gamma distribution model performed between the smaller and larger image stack, where the Gamma distribution model performed better for the larger stack, which could point to even better fit to the distribution model if an even larger image stack was used.

Keywords: SAR, Image-stack, TanDEM-X, TerraSAR-X, Anderson-Darling, Distribution model, Krycklan

Acknowledgements and special thanks

Patrik Dammert and Gary Smith-Jonforsen, both at Saab AB, for tutoring me and always being available for discussions and giving me their greatly appreciated point of view.
Lars Ulander, Chalmers, for providing me with the opportunity to work on this master thesis.
Maciej Soja, MJ Soja Consulting, for providing matched SLC data, which saved many hours of time for the project.
TanDEM-X and TerraSAR-X data have been provided by the German Aerospace Center (DLR) through a research agreement with Chalmers University of Technology.
Many heartfelt thanks to my loving wife Fatima, who has given me the time and resources needed at home to allow me to conduct my work. Countless times has your smile and love pushed me through any difficult and frustrating situations that have occurred.

Adam Hessing, Gothenburg, June 2020

List of Abbrevations

AD Anderson-Darling.
CDF Cumulative Distribution Function.
EDF Empirical Distribution Function.
EM Electromagnetic.
MLE Maximum Likelihood Estimation.
PDF Probability Density Function.
SAR Synthetic Aperture Radar.
SLC Single Look Complex.

Contents

List of Figures

List of Tables

1
Introduction

Synthetic Aperture Radar (SAR) provides the ability to generate high resolution images of the Earth's surface [2]. Looking at and modeling the distributions of the data spatially have been well covered in the literature for quite some time [2], but recent satellite developments and projects will provide a lot of high quality as well as a high quantity of SAR data [3], which enable the analysis of the SAR images in time as well. Looking at a large number of different SAR images, called an image stack, taken of the same surface area but at different times, provides the ability to analyze the distributions of the data, not only spatially but more importantly in time, which is not well covered in the literature and is what this thesis will focus on. The analysis is done on two different image stacks of intensity SAR images which have been matched, so that every pixel on one SAR image has the same position for every image in the image stack.
The aim of the thesis is to investigate the validity of different distribution functions to describe the variations between images for each pixel in the entire stack. Also differences which may depend on land-cover type are investigated. This enables the data to be observed in time instead of an area from the same image. One of the reasons this type of work would be interesting is that it might allow for improved and effective change detection algorithms when using temporal data instead of spatial data. The reason for this is that when spatially looking at an area there could be several different distributions that will be taken into account while a temporal approach would only use a pixel from every image within the image stack and thus not mixing different data from different surface areas. The intensity values can have a larger variation when looking at spatial data samples compared to temporal data samples, which could mean that a change detection test that uses temporal data has the possibility to be much more sensitive and would allow detection of smaller targets. The aim of this thesis, to model the data distributions, is an important step towards achieving such change detection tests.

2

Theory

2.1 Spatial and temporal definition

Throughout the report the terms *spatial* and *temporal* are used. Figure 2.1 illustrates the meaning of the terms. By spatial it means looking at a group of pixels from the same SAR image, while temporal means that the data is located at one specific pixel position through the entire image stack.

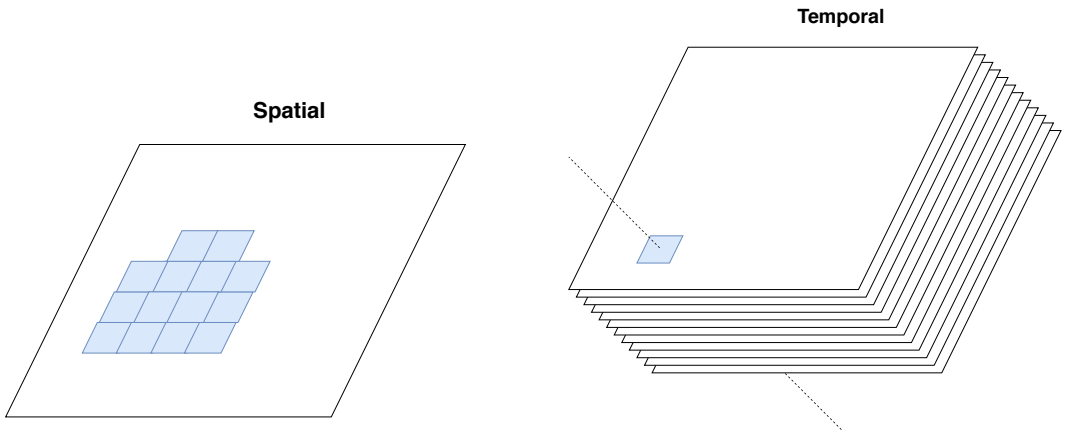

Figure 2.1: The blue squares corresponds to chosen pixels in two different scenarios. The spatial refers to a cluster of pixels in the same SAR image while the temporal refers to one pixel position through the entire image stack.

2.2 SAR introduction

The basics of any radar technology is that electromagnetic (EM) signals are transmitted and the reflected echoes (backscattering) are intercepted, processed and analyzed [4]. The backscattering properties depends on the frequency of the transmitted EM waves which have led to the introduction of frequency bands to easier classify different radar system [5].

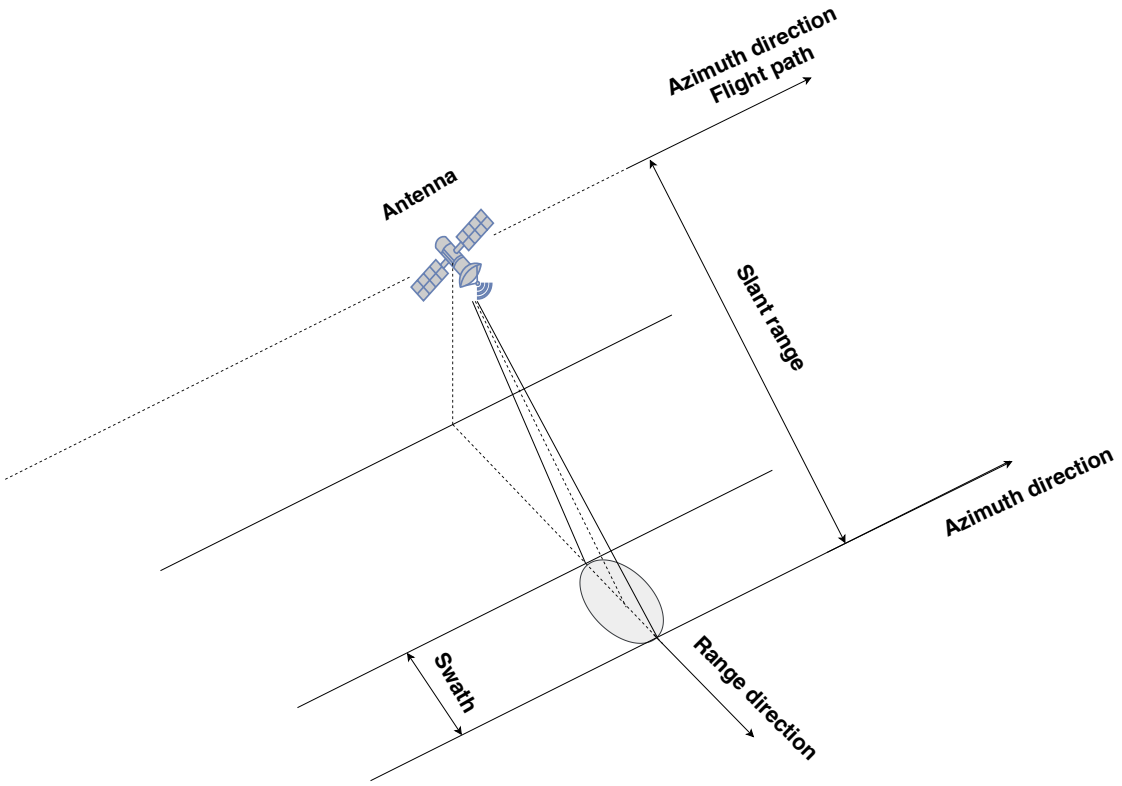

Figure 2.2: Shows the geometry and terminology of a typical SAR system. Where azimuth is the flight direction of the antenna, range direction is the direction perpendicular to the azimuth and slant range is the distance between the antenna and and the ground of which the data is collected.

Some of the terminology used for SAR is illustrated in figure 2.2. The satellites flight path is called *azimuth* and perpendicular to the azimuth is called *range direction*, which is the direction the antenna is pointed towards. The distance between the antenna straight track and the point on the Earth's surface that the EM signal is backscattered from is called *slant range*. The *swath* width refers to the strip of the earth's surface that data are collected from the antenna.
The strength of SAR is the ability to synthesize a larger aperture than the real aperture of the antenna. By advanced signal processing a simulated larger synthetic aperture can be created, taking advantage of the phase information from a number of consecutive backscattered signals. This allows for improved SAR image resolution that otherwise would require a much larger physical antenna aperture [5].

2.2.1 Speckle

Analyzing the SAR intensity data as an image makes it possible to distinguish shapes, regions, certain objects, lines and the overall structure of the image. Looking closer at the image, a noise like effect is noticeable. Focusing on a homogeneous area of the image it is noticeable that the intensity can vary quite a lot between adjacent pixels. This noise like effect is called *speckle* and to clarify it is not actual noise but is a real electromagnetic measurement which can be exploited in other uses of SAR

imagery [2]. The speckle effect is present due to several small backscattering objects within a resolution cell that is smaller than the resolution of the image and thus the total backscatter of that cell is the sum of each small backscatter which can be heightened or lowered by constructive or destructive interference.

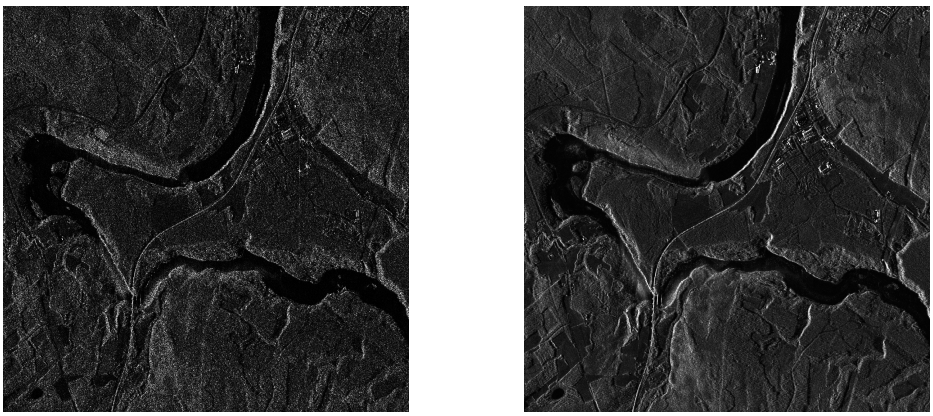

Figure 2.3: SAR image of the same surface area where the left side shows the speckle effect and the right side a speckle reduced image.

The left side of figure 2.3 shows the speckle effect and there are a number of ways to reduce this effect to improve the visibility of the image [6]. The right side of 2.3 shows a speckle reduced SAR image of the same area as the left side in the same figure. A simple speckle reduction technique has been used by averaging the pixel intensity over all images in the image stack. Each pixel's intensity is calculated by

$$I_{SpeckleReduced} = \frac{1}{N} \sum_{n=1}^{N} I_n, \tag{2.1}$$

where I is the intensity, n is the index of one image in the image stack and N is the total number of images in the image stack. In this thesis a speckle reduced image has been used to compare the SAR images to a real map in an effort to characterize what type of surface areas are visible in the SAR images. The speckle reduced image has solely been used as a visual aid but not for any analysis of the intensity data.

2.3 SAR Image data

The SAR data provided for this thesis are acquired by a X-band twin-satellite system, TanDEM-X, which generates complex data consisting of amplitude and phase. The TanDEM-X system consists of two almost identical satellites in a tight formation [7]. Since it is a twin-satellite system every SAR image is a part of an image pair which have been taken very close to each other in time, which would mean that the data within an image pair would be more correlated than outside of the

image pair [7]. The data that's been used in this thesis is initially acquired by the satellites with the intent to investigate tree heights and thus the satellites have a spatial baseline which is adjusted to better capture tree heights. Because of this spatial baseline the image pairs are expected to be partially correlated. The spatial baseline is defined as the perpendicular distance between the satellites orbits [5, 7]. The SAR data has been retrieved of an area approximately 50 km north-west of Umeå in northern Sweden. The surface areas from the two different image stacks overlap in certain areas, which can be seen in figure 2.4.

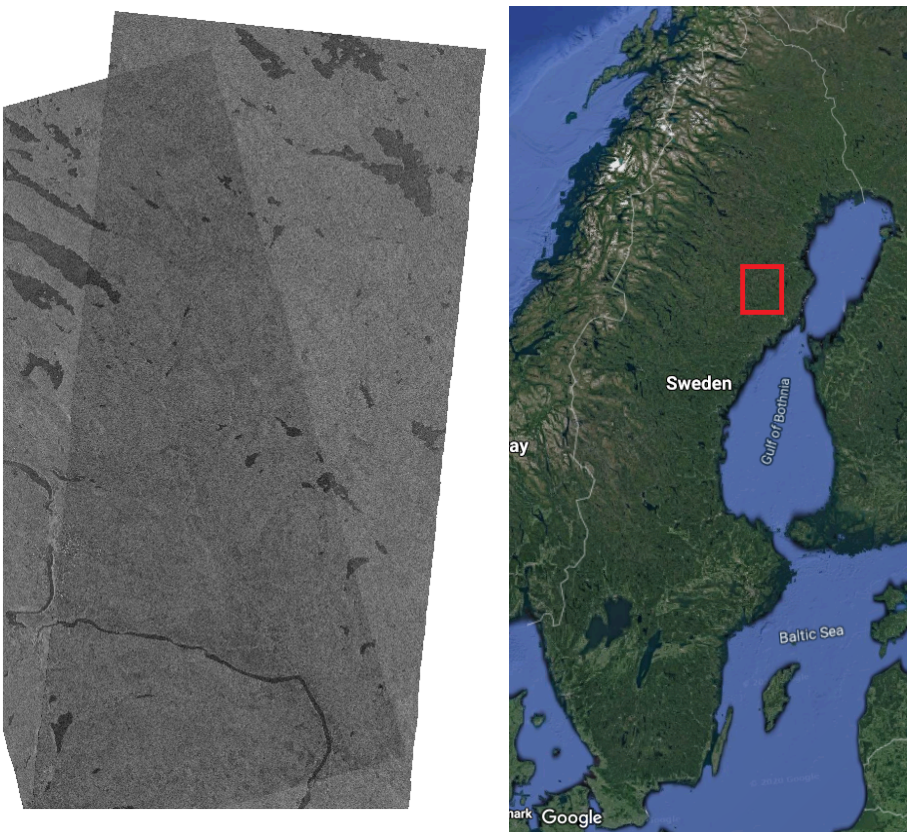

Figure 2.4: Figure showing the overlapping of the two image stacks. The left tilted part shows the area of image stack 1 and the right tilted part shows the area of image stack 2. The right side of the image showing which part of Sweden the data is collected from.[1]

The complex data have been calculated to intensity data according to

$$I_k = |Z_k|^2, \tag{2.2}$$

where k is the index for each specific pixel and Z is the complex SAR data related to that pixel.
There are two different image stacks that have been studied, the first image stack has 14 image pairs with a total of 28 images and the second image stack contain 32 image pairs of total 64 images [8]. The first image stack is taken in ascending orbit while the second image stack has been taken in descending orbit. Even though the both image stacks contain many of the same surface areas it would be unwise

to add them together and analyze both at the same time, since the image stacks differ in resolution cell sizes and thus would have different information within each pixel. Also the different image geometry means that the same objects may appear different between the image stacks due to the direction from which they are viewed.

Table 2.1: Detailed information of the SAR image stacks.

	Image Stack 1	**Image Stack 2**
# Images	28	64
# Image pairs	14	32
Center frequency [GHz]	9.65	9.65
Image size [pixels]	19368 x 15678	20646 x 13798
Azimuth resolution [m]	3.3	6.6
Slant range resolution [m]	1.2	1.2
Incidence angle [degrees]	40.47 - 40.66	44.08 - 44.14
Polarization	VV	VV
Azimuth pixel size [m]	1.89	2.57
Ground range pixel size [m]	1.36	0.91

2.4 Candidate distribution models

The spatial distributions have been investigated in [2] for forest and field areas but with the Kolmogorov–Smirnov test which is an alternate goodness-of-fit test than what is used in this thesis [9]. The results in [2] showed that the K-distribution was the best spatial distribution fit for forest areas and for the field area, the Weibull distribution had the best fit.

Since the focus of this thesis is to investigate the purely temporal distributions of intensity SAR data, the reasoning on which distributions to test within this thesis are based on the spatial distributions which already is covered in literature e.g. [2]. The K distribution has unfortunately not been introduced in this thesis due to difficulties in integrating it into the statistical goodness-of-fit test that has been used. The K distribution on the other hand has previously been found to be a useful model for SAR data and thus it's unfortunate that the K distribution was not able to be a part of this thesis [10]. The candidate distribution models the SAR data have been tested against can be seen in table 2.2 with its corresponding probability density function (PDF) defined.

Table 2.2: List of distributions that the intensity SAR data have been tested against.

Distribution	**PDF**	**Parameters**
Normal	$\frac{1}{\sigma\sqrt{2\pi}} \exp\left(-\frac{(x-\mu)^2}{2\sigma^2}\right)$	μ = mean, σ = standard deviation
Extreme value	$\sigma^{-1} \exp\left(\frac{x-\mu}{\sigma}\right) \exp\left(-\exp\left(\frac{x-\mu}{\sigma}\right)\right)$	μ = location, σ = scale
Gamma	$\frac{1}{\Gamma(\alpha)\beta^\alpha} x^{\alpha-1} \exp\left(-\frac{x}{\beta}\right)$	α = shape, β = scale
Exponential	$\mu \exp\left(-\mu x\right)$	$\mu = 1/\text{mean}$
Rician	$\frac{x}{\sigma^2} \exp\left(\frac{-(x^2+s^2)}{2\sigma^2}\right) I_0\left(\frac{xs}{\sigma^2}\right)$	s = noncentrality, σ = scale
Rayleigh	$\frac{x}{b^2} \exp\left(-\frac{x}{2b^2}\right)$	b = scale
Lognormal	$\frac{1}{x\sigma\sqrt{2\pi}} \exp\left(-\frac{(\ln x-\mu)^2}{2\sigma^2}\right)$	μ = mean of $ln(x)$, σ = standard deviation of $ln(x)$
Weibull	$\frac{b}{a}\left(\frac{x}{a}\right)^{b-1} \exp\left(-\left(\frac{x}{a}\right)^b\right)$	a = scale, b = shape

Figure 2.5 shows examples of how the distributions look like for a few selected distributions from table 2.2. The Gamma and Exponential distribution models are related where the Gamma distribution is a special case of the Exponential distribution. If the Gamma parameter, α, is equal to 1 that gamma distribution is equal to an Exponential distribution with μ parameter equal to $\frac{1}{\beta}$.
And the Gamma distribution is a special case of the Exponential distribution, with shape parameter = 1, which could be a reason why the Gamma distribution performs well for intensity data.

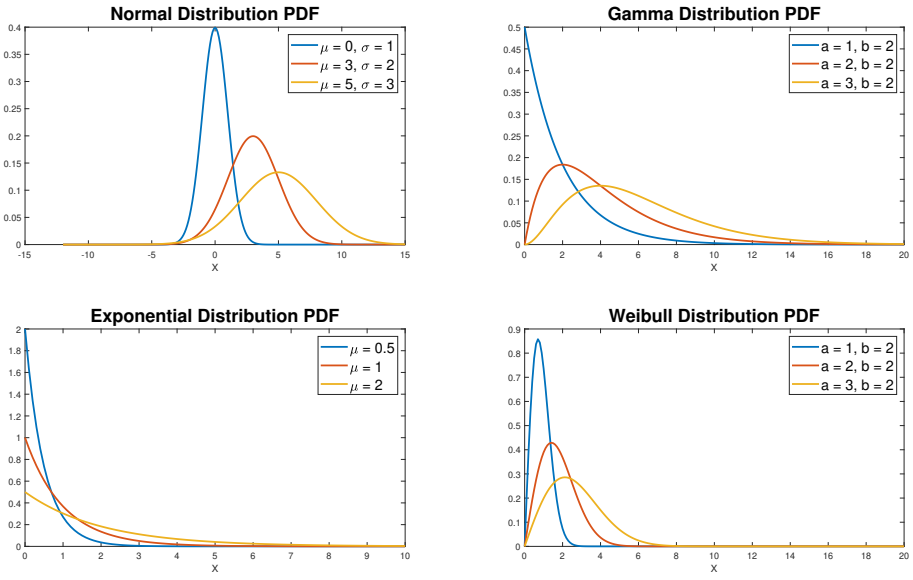

Figure 2.5: Showing PDFs of four of the target distributions listed in table 2.2, with three different sets of parameter values.

The aim is to investigate if, and how well the intensity SAR data match these different distributions.

2.5 Anderson-Darling Test

The Anderson-Darling (AD) test is a statistical goodness-of-fit test whether an independent sample set of data fits to a given probability distribution model. As mentioned in section 2.3 the data used in this thesis is not completely independent, although with the effect of speckle the intensity values can have a large variation even between the image pairs that it's considered sufficient for the AD-test. The test results in whether the sample set of data is rejected or not against the null hypothesis, H_0. If H_0 is rejected the sample data is not considered to be a part of the target distribution. The test statistic, introduced in [11] is given by

$$A^2 = n \int_{-\infty}^{\infty} (F_n(x) - F(x))^2 w(x) dF(x), \tag{2.3}$$

where n is the number of elements in the sample data, $F_n(x)$ is the Empirical Distribution Function (EDF), $F(x)$ is the theoretical CDF and $w(x)$ is a weighting function. The Anderson-Darling weight function is given by

$$w(x) = F(x)(1 - F(x)), \tag{2.4}$$

and is set to give more weight on the observations at the tails of the distribution. An alternative way of calculating the test statistic given in equation 2.3, it's possible to use the following formula

$$A^2 = -n - \frac{1}{n} \sum_{i=1}^{n} (2i - 1)[ln(F(Y_i)) + ln(1 - F(Y_{n+1-i}))], \tag{2.5}$$

where Y_i is the ordered sample data set from lowest to highest value [12, 13]. The test statistic A^2 is then compared to the distributions critical value τ to reject the null hypothesis, H_0 or not. If the test statistic is larger than the critical value according to $A^2 > \tau$ the null hypothesis is rejected and the sample data set is not considered to come from the target distribution.
The critical values depend on which distribution and a chosen significance level, α, that are used in the AD test. Some of the critical values for corresponding distribution and significance level α are covered in [14] while other values for τ, together with a probability value of how probable it is that the data fits to the target distribution, can be calculated by a method according to [15]. The probability value have been used to compare which target distribution model that was considered the best where the higher probability was considered the better result.

2.5.1 Parameter estimation

Since the distribution of the sample data isn't known the parameters for each target distribution needs to be estimated. Each of the parameters given in table 2.2 are estimated by Maximum Likelihood estimation (MLE), which provides a parameter estimation that maximizes the likelihood of the current data set that most likely fits the statistical model [16, 17]. The MLE is able to estimate parameters sufficiently as the sample size goes to infinity [18], but since that is rarely the case in real problems and this thesis in not an exception, it is expected that the MLE estimation is not

perfect and may have an negative impact on the results, since according to equation 2.3 the A-D statistic, A^2, value is calculated bu the difference between the EDF and the theoretical CDF. If the parameter estimation is incorrect that would mean that the theoretical CDF used in equation 2.3 would not be the true distribution model for that specific EDF. This however is a general issue for all methods used for parameter estimation and is difficult to avoid with such a limited number of data samples.

3
Methods

Most of the practical work conducted within this thesis have been done using the Matlab software [19] and the following section will explain in further detail how the project has been conducted.

3.1 Preparation of the SLC SAR data

As stated in section 2.3 the SAR data that have been provided to this project is complex SAR data, which have been calculated to intensity data, according to equation 2.2. The data have then been separated into five different surface area types, shown in table 3.1, to be able to compare the data in a more controlled manner and to be able to compare spatial distributions to the temporal distributions within the same type of surface area.

Table 3.1: Shows which types of surface areas and how many different parts of these areas that have been investigated from both image stacks.

Area types	**#of parts/area type**	**Description**
Lake	4	An area composed of water.
Forest	4	An area composed of woodland.
Clear Cut	4	A deforested area.
Field	4	A plain grassland area.
Structure	4	An area mainly composed of buildings.

3.1.1 Speckle reduction

As mentioned in section 2.2.1 there is a speckle effect in the SLC images which worsens the quality and the ability to visually analyze the images. To reduce this speckle we take advantage of the fact that the image stacks contain a large number of images taken over the same at different times. This makes the possibility to, for each pixel location in the stack, average over all intensity values for that pixel position according to equation 2.1. This has been used to visually inspect and identify different types of surface areas in more detail.

3.1.2 Selecting the different surface areas

Selecting the different surface areas was done by comparing the speckle reduced SAR image for each image stack with the same areas in Google Maps [20], to visually inspect that the surface area located in the SAR images corresponds to one of the area types given in table 3.1. Four different areas of each area type specified in table 3.1 was selected from both of the image stacks.

3.1.2.1 Matlab function: roipoly()

The Matlab function *roipoly* was used to cut out, chosen by the means explained in section 3.1.2, the different parts from the larger SAR data matrices. The roipoly-function enables the user to create a polygon from a larger image and reduce it to a smaller image i.e. the different surface area types given in table 3.1. Figure 3.1 shows how it's possible to reduce a larger image to a smaller image only containing the data that is found of interest, which in this example is shown of a lake.

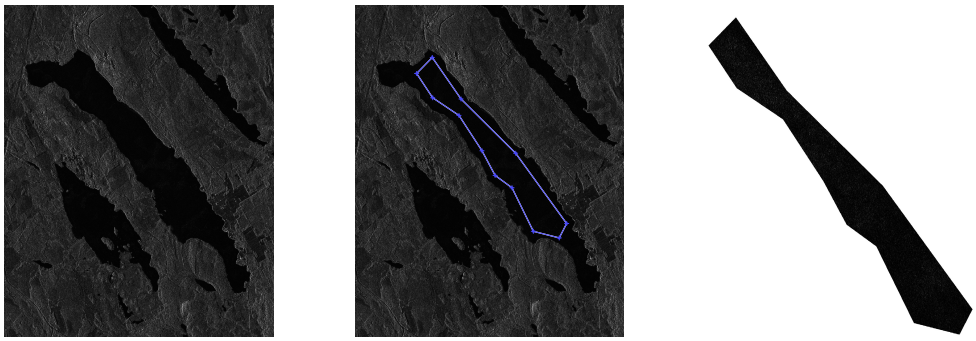

Figure 3.1: Shows how the Matlab function roipoly() reduces a larger image to a smaller image within the user specified blue polygon.

3.2 Seasonal variations

Since the image stacks contain a large number of different images from different times during the year it would be of interest to see if there are any seasonal variations in the images. This can be done by calculating the mean of an area for each image in the image stack as well as the standard deviation and then create a plot where it's possible to chronologically see if there are variations in the mean depending on which time of the year the SAR image has been taken.

3.3 Investigating distributions models against data

The investigation of the distribution models have been done both visually and as a statistical test described in section 2.5. The visual inspection is mainly done on the spatial distributions over the different areas stated in table 3.1 to try to determine if there is a difference in distribution depending on surface area type.

3.3.1 Visual inspection by histograms

A visual inspection of the distribution can easily be made by creating a histogram of the data and look at the shape of the histogram if it matches one of the target distributions in table 2.2. This type of visual inspection is mostly to give a hunch on what distributions might be most prominent for the actual test later on.

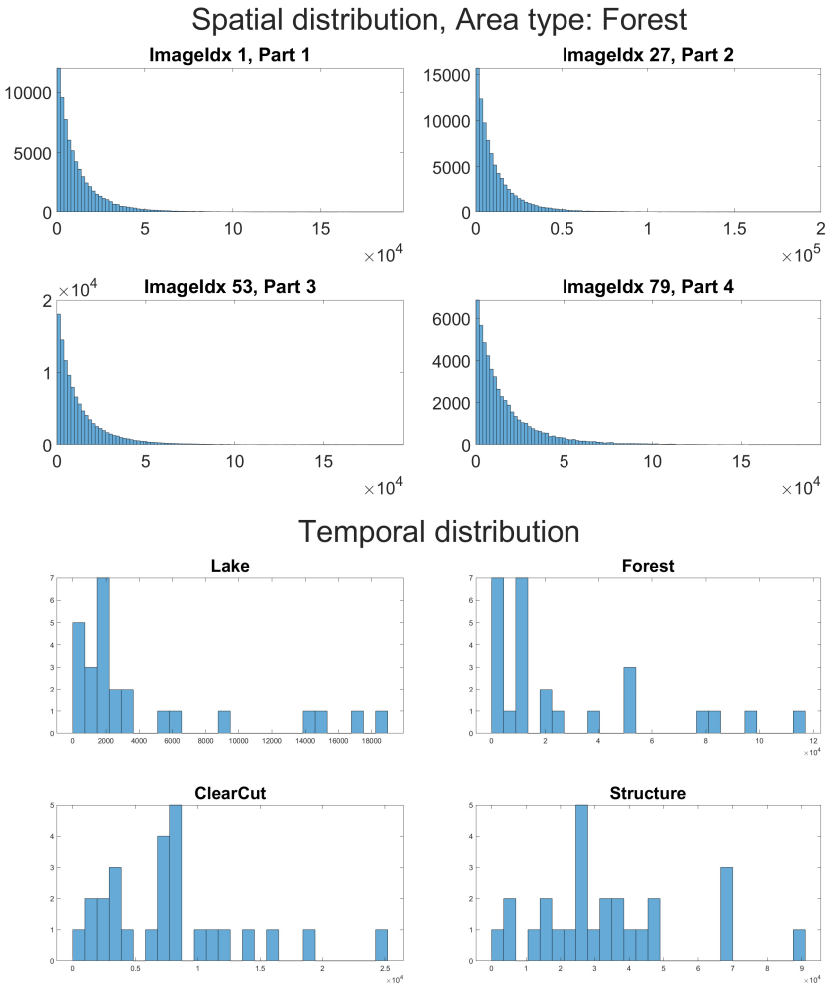

Figure 3.2: The left side shows histograms of spatial data samples from one specific image. The right side shows histograms of temporal data samples from one pixel position through the whole image stack.

As an example, figure 3.2 shows histograms of both spatial data as well as temporal data. The top four plots in figure 3.2 shows the distribution of a spatial data set, where it's possible to see a distinct shape of the histogram. Comparing the histogram to figure 2.5 it's possible to assume that either a Gamma or Exponential distribution could be a good fit to the data. The visual inspection of the temporal histograms, shown in the lower 4 plots in figure 3.2, is much more difficult since the amount of data samples are so few. It's the depth of the image stack that sets the limit for the temporal investigation. A visual inspection of such a low number of images is

not realistic and therefore all target distributions could be possible for the temporal case.

3.3.2 Anderson-Darling Test

The A-D test calculates a test statistic value from the data samples by comparing its EDF to a target distributions CDF as stated in section 2.5. The test statistic is calculated using a function in MATLAB called *adtest*. The function calculates the test statistic according to equation 2.5. A significance level of $\alpha = 0.05$ has been chosen to compare the test statistic against for rejecting the null hypotheses, H_0 or not, which is a common value for α for A-D tests [21]. The critical value, τ is calculated according to section 2.5.

4

Results

4.1 Image matching

A visual investigation of the images in the image stacks was made to make sure that each pixel on each image in the image stack corresponded to the same surface area. By letting the images be on top of each other and flip back and forth between the images it shows if the pixels were aligned or not. There was one image pair in the first image stack that was found to not be matched to the other images in the stack. It appeared to have a different resolution in azimuth range. The solution to this problem was to remove this image from the image stack for the rest of the process. This was very unfortunate since the first image stack, which is already at half the sample size of the second image stack, became even smaller. Figure 4.1 shows the difference between three different images from the first image stack where the matching issue appears for one of the images. An area with a stable backscatter object was chosen to perform the visual inspection.

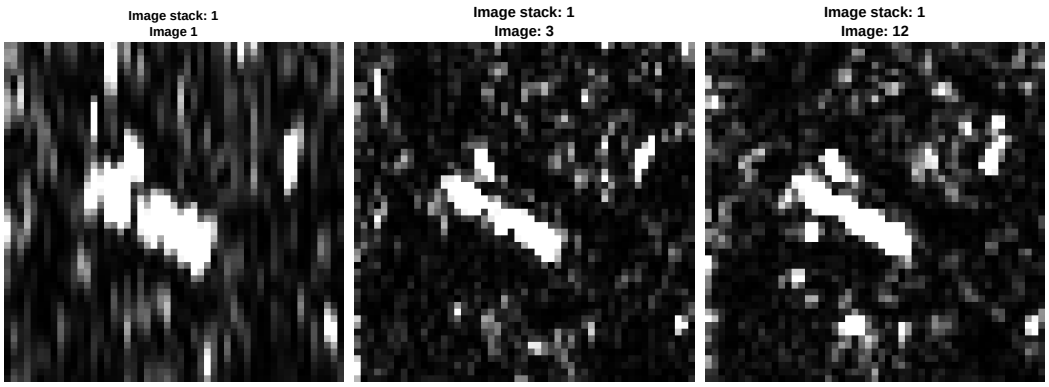

Figure 4.1: Examples of how the matching was done with the images. The left image shows one image which proved not to be matched with the other images due to a resolution difference in azimuth. The azimuth resolution in the left image has been calculated to approximately 9 m instead of 3.3 m for the rest of the images in image stack 1. The left image was removed from the first image stack.

In the second image stack all 64 images was considered to be well matched after going through the same visual inspection as the first image stack.

4.2 Seasonal variations

According to appendix A the SAR images have been taken at different times over several years. As could be expected a seasonal difference in mean intensity can be observed in figure 4.2.

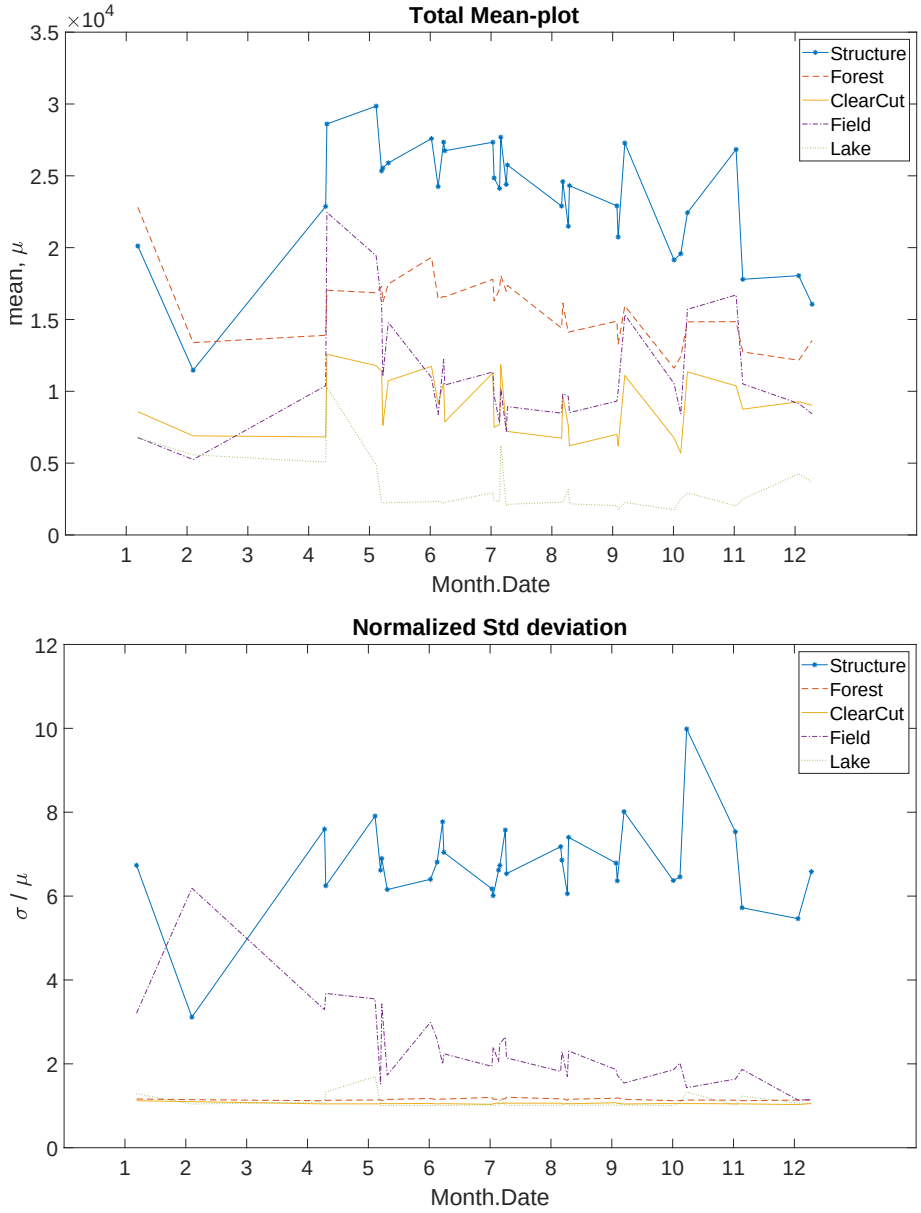

Figure 4.2: Top image showing mean of the intensity for each area type given in table 3.1. Bottom image showing the corresponding normalized standard deviation, σ. Only one image from each image pair is included in the plot due to high correlation in mean values within each pair.

The mean intensity is generally lower in the months of winter which could possibly be explained by ice and snow which can provide a lower backscattering depending on the surface roughness and moistness [22]. It's important to note also that the

variations could also be due to calibration errors since some of the images are taken years apart. Taking into account data of the temperature, seen in figure 4.3 during these periods you can see that it corresponds well with that the wetness and the probability of snow and ice during winter months could be a contribution factor of the difference in mean intensity [23, 24].

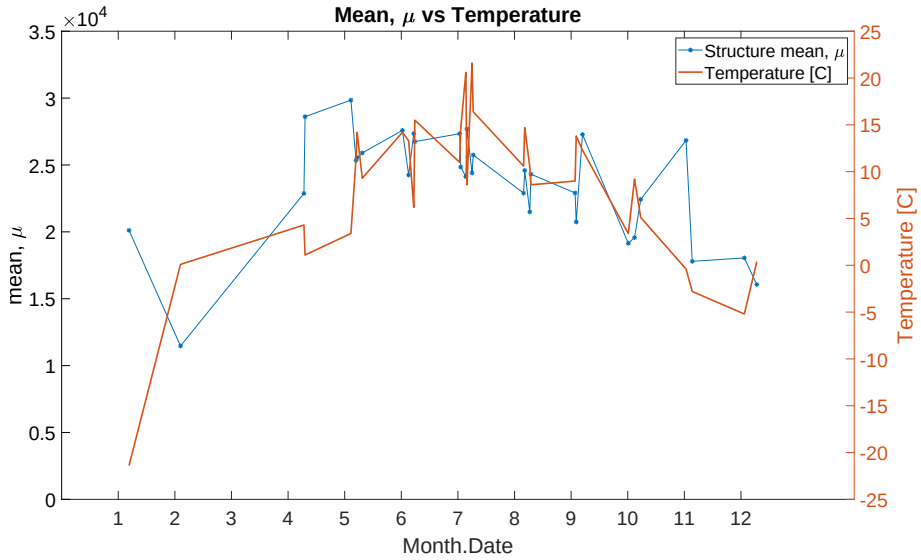

Figure 4.3: Showing the correlation between the temperature and the intensity of the SAR images.

4.3 Anderson-Darling test results

After performing the Anderson-Darling test on all pixels for each of the different area types, it was made clear that the Gamma distribution stood out against the rest of the target distributions stated in table 2.2. Statistical results of the A-D test have been presented in section 4.3.1 and more visual interpretations of the A-D test results have been made in section 4.3.2.

4.3.1 Statistical results of the A-D test

The sample data is shown to be best fitted to the Gamma distribution in a clear majority of the cases, indifferent of area type. The Gamma distribution performs slightly better on forest and clear cut areas while it performs a bit worse on the lake surface area type, as can be seen in table 4.1 for image stack 1 and in table 4.2 for image stack 2. The rejected H_0 is summarized in the first line in the tables independent of which target distribution model the null hypothesis got rejected. The decision on which distribution got the best result of the A-D test is based on the probability value calculated in the A-D test.

Table 4.1: For Image Stack 1 , this table shows percentages of which distribution got the best result from the AD-test for each area type.

Distribution	**Lake**[%]	**Forest**[%]	**Clear Cut**[%]	**Field**[%]	**Structure**[%]
H_0 Rejected	01.04	00.04	00.15	00.09	00.95
Normal	00.08	00.62	00.68	00.42	01.33
Extreme value	00.00	00.05	00.05	00.03	00.49
Gamma	75.60	91.40	88.94	88.65	85.63
Exponential	00.00	00.00	00.00	00.00	00.01
Rician	00.00	00.00	00.00	00.00	00.00
Rayleigh	00.01	00.25	00.29	00.16	01.06
Lognormal	22.90	07.57	09.80	10.55	10.41
Weibull	00.37	00.07	00.09	00.10	00.12

Table 4.2: For Image Stack 2 , this table shows percentages of which distribution got the best result from the AD-test for each area type.

Distribution	**Lake**[%]	**Forest**[%]	**Clear Cut**[%]	**Field**[%]	**Structure**[%]
H_0 Rejected	01.19	00.01	00.00	00.11	01.26
Normal	00.00	00.01	00.01	00.01	00.68
Extreme value	00.00	00.00	00.00	00.00	00.16
Gamma	83.78	96.55	96.49	91.28	92.07
Exponential	00.01	00.02	00.02	00.01	00.01
Rician	00.00	00.00	00.00	00.00	00.00
Rayleigh	00.00	00.00	00.00	00.00	00.00
Lognormal	14.58	03.34	03.39	08.31	05.56
Weibull	00.44	00.07	00.09	00.28	00.26

What needs to be clarified on the results stated in table 4.1 and table 4.2 is that this percentage only shows the distributions that got the best result in the A-D test but not how certain the test have been on a correct result, i.e. how close it was for the null hypothesis, H_0, to be rejected. Also the tables shows only which distribution models that got the best result but not if there were other distribution models that gave reasonable results as well.

Table 4.3 and 4.4 shows how many percent of each distribution that passed the A-D test, i.e. where the null hypotheses, H_0 didn't get rejected. The tables show that even though the Gamma distribution is clearly the distribution that passed the test most frequently, there was still three more distributions, the exponential, lognormal and weibull distributions, that had a high pass rate as well.

Table 4.3: For Image Stack 1 , this table shows percentages of how many pixel positions passed the A-D test, i.e. didn't get H_0 rejected, for each distribution.

Distribution	**Lake**[%]	**Forest**[%]	**Clear Cut**[%]	**Field**[%]	**Structure**[%]
Normal	02.71	12.25	11.93	09.55	14.40
Extreme value	00.21	01.60	01.65	01.19	03.20
Gamma	98.31	99.95	99.82	99.88	98.66
Exponential	66.00	87.94	83.48	82.60	77.44
Rician	00.00	00.00	00.00	00.00	00.00
Rayleigh	01.41	08.72	08.96	06.34	12.75
Lognormal	78.27	66.56	67.79	69.85	65.99
Weibull	83.64	91.88	89.49	90.55	86.21

Table 4.4: For Image Stack 2 , this table shows percentages of how many pixel positions passed the A-D test, i.e. didn't get H_0 rejected, for each distribution.

Distribution	**Lake**[%]	**Forest**[%]	**Clear Cut**[%]	**Field**[%]	**Structure**[%]
Normal	00.00	00.07	00.07	00.03	01.42
Extreme value	00.00	00.00	00.00	00.01	00.27
Gamma	97.51	99.97	99.99	99.73	97.65
Exponential	63.90	89.40	89.27	76.76	79.81
Rician	00.00	00.00	00.00	00.00	00.00
Rayleigh	00.00	00.00	00.00	00.00	00.00
Lognormal	49.57	31.78	32.22	41.85	33.54
Weibull	79.74	92.46	93.22	88.67	87.35

4.3.1.1 Parameter estimation

Each target distribution has it's own set of parameters that have been estimated from the SAR data as explained in section 2.5.1. As previously mentioned the Gamma distribution is a special case of the Exponential distribution. When the Gamma parameter $\alpha = 1$, the Gamma distribution fits an Exponential distribution. As can be seen in table 4.4 and 4.3 both the Gamma distribution and the Exponential distribution has a high pass rate. Figure 4.4 shows box plots for the estimated α values, from the SAR data, for the Gamma distribution model. The blue box in the box plots contain 50% of the estimated values.

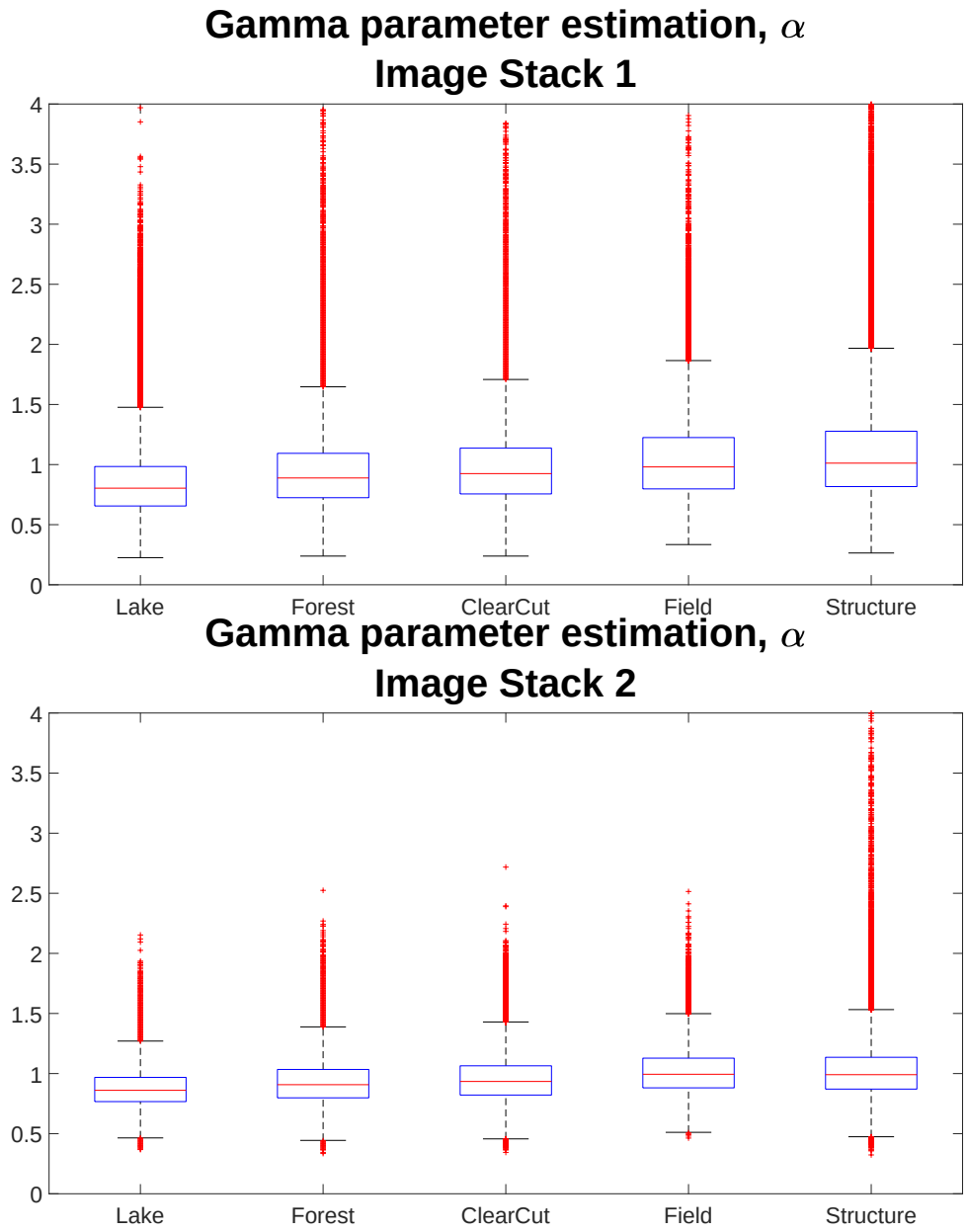

Figure 4.4: The estimated values for the Gamma parameter α shown as box-plots. 50% of the estimated values is contained within the blue boxes for each surface area type.

The information of how close to 1 the estimated α parameters are it is not surprising that also the Exponential had a high pass rate in the A-D test, even though the pass rate was not as high as the Gamma distribution model.

4.3.2 Visual color maps of the A-D test

Color maps have been created where each distribution has been assigned a specific color. The color of each pixel is defined by the color of the distribution which provided the best fit. The color maps have been used to more easily compare the different results of the AD-test and to see if there are any spatial patterns present

depending on which distribution had the highest result of the test. Taken into account the information stated in the tables of section 4.3.1, the following sections will mostly focus on the distributions that's proved to be most interesting. More extensive information on the rest of the distributions can be found in appendix B.

4.3.2.1 Image stack 1

As for all area types figure 4.5 clearly shows that the Gamma distribution got the best result for most of the pixels. For the lake area type it's possible to see a pattern for the Lognormal distribution in *Part 1* and *Part 2*. These patterns match the shape of where ice is located for one image pair in the image stack.

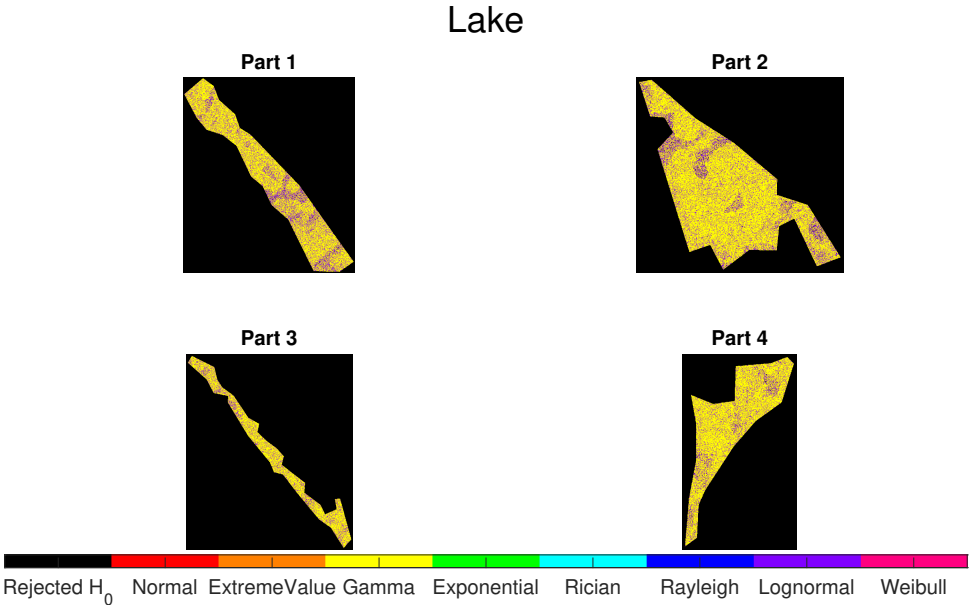

Figure 4.5: The yellow coded Gamma distribution is the most prominent distribution for forest areas.

This means that for as little as 2 out of a total 26 images in image stack 1 allows the Lognormal distribution to perform better than the Gamma distribution at certain conditions, shown in figure 4.6.

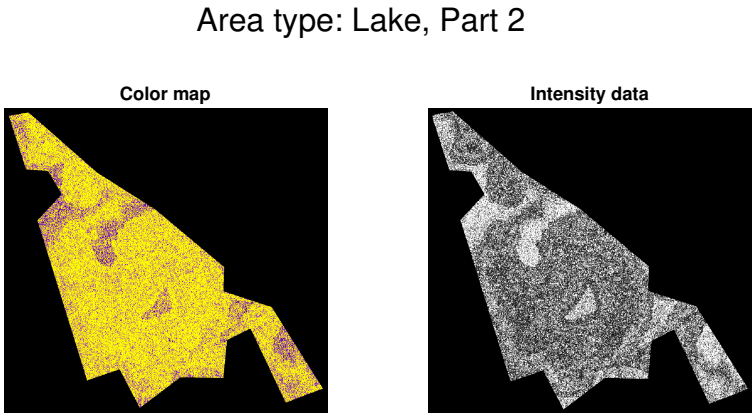

Figure 4.6: The lognormal (purple) distribution comes out on top when ice (white patches) is present for 2 out of 26 images.

There weren't many more interesting results for image stack 1, but to see the rest of the color plots for the first image stack, see appendix B.

4.3.2.2 Image stack 2

It can be seen in figure 4.7 and figure 4.8 the Gamma distribution have shown to be fitted best to both the Forest data and the Lake data. This is also true for all different types of areas, just like for image stack 1, given in table 3.1 although with a varying degree of how often the Gamma distribution was the best fit.

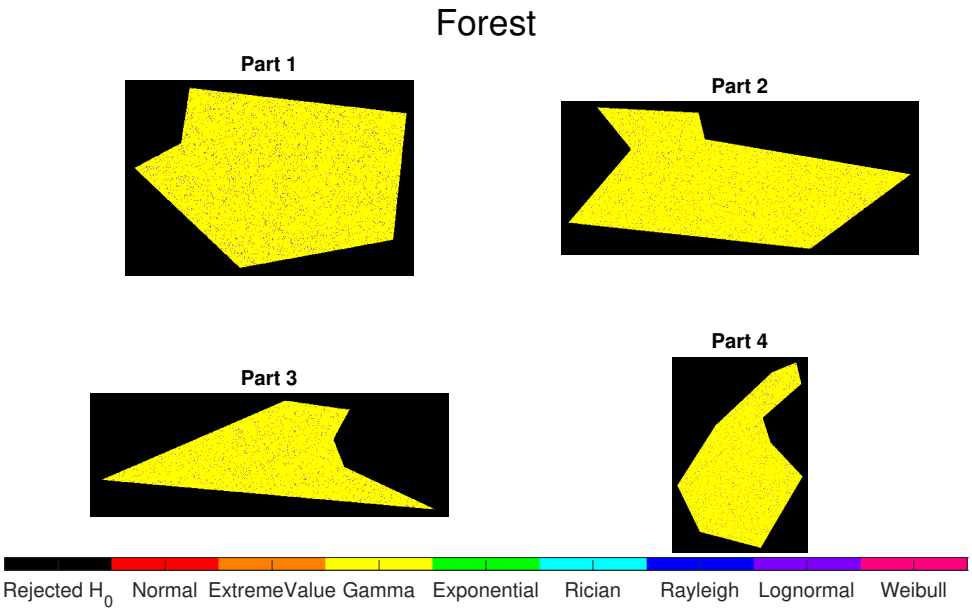

Figure 4.7: The yellow coded Gamma distribution is the most prominent distribution for forest areas.

In figure 4.7 it is shown that approximately 97% of the pixels of the forest area type had Gamma as the best fit to the data.

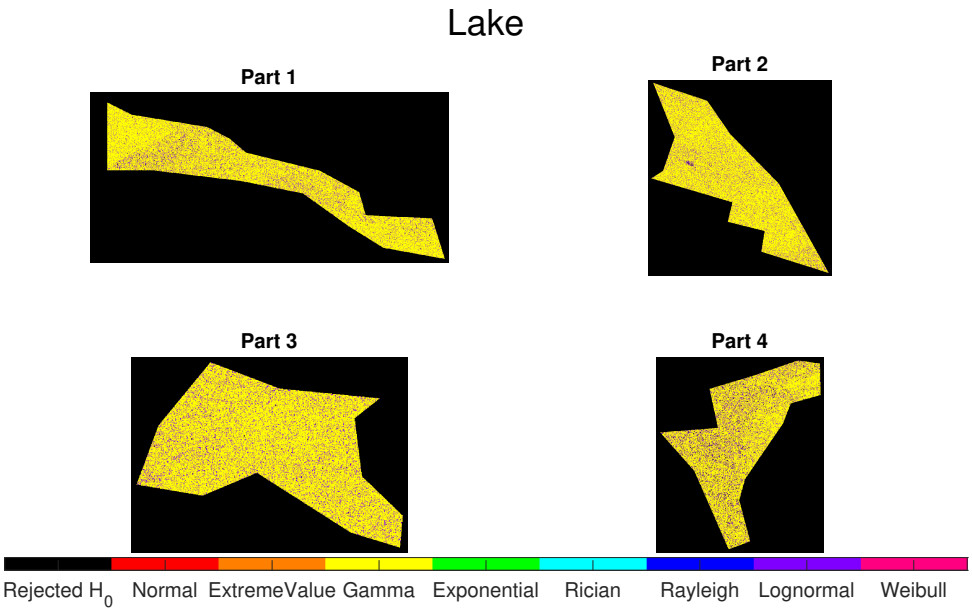

Figure 4.8: Gamma is the most recognized distribution

In figure 4.8 the Gamma distribution is shown to be fitted best at 84%, still being the best fit for the most pixels, but not as high as for the forest areas. All area types have in common that the Gamma distribution has the best fit in a clear majority of cases. All area types, beside the structure area type, have in common that there is no particular pattern for how the different distributions are located in the color maps.

The color map for the structure area type, figure 4.9, shows something interesting. It clearly shows a pattern where the Gamma distribution fails and other distributions shows up in small clusters. Interestingly these clusters of non-Gamma positions are located where buildings seem to be located when looking at the SAR intensity data, seen in figure 4.10.

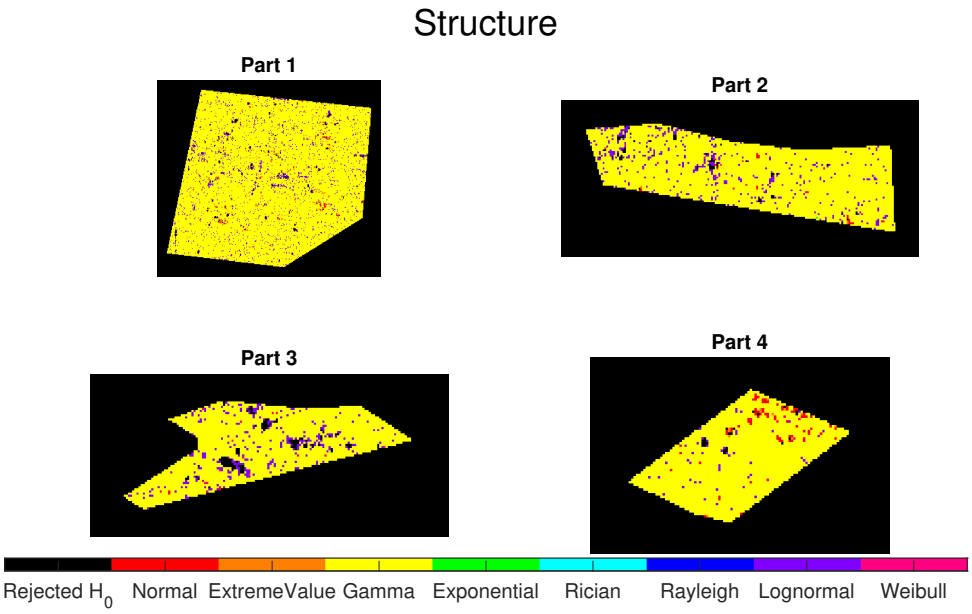

Figure 4.9: The same as in the other regions but here there is also a prominent outline for where some buildings are present.

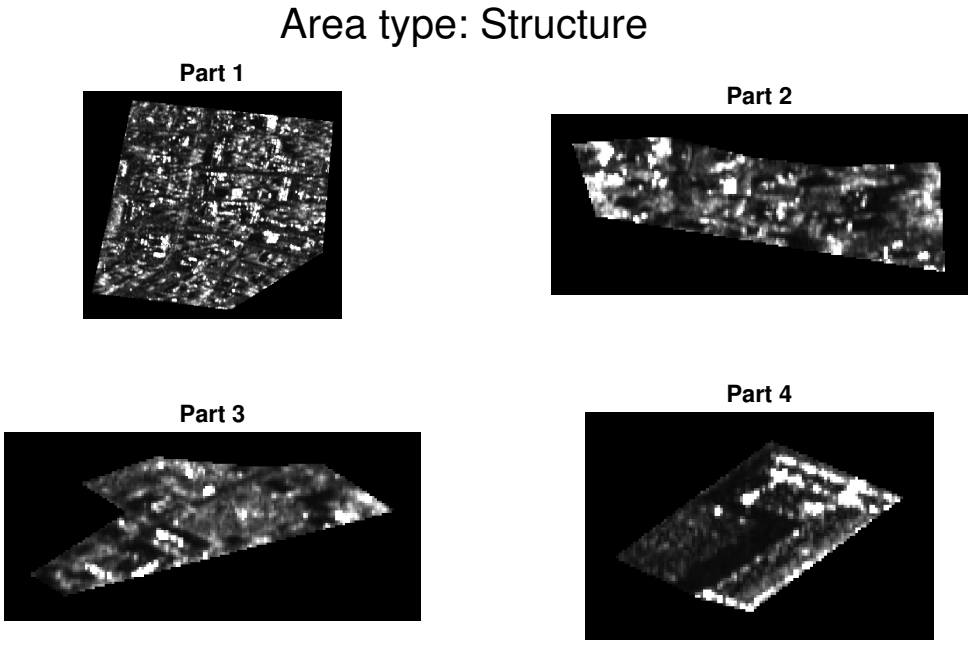

Figure 4.10: SAR intensity image of the same surface area as the structure color maps.

4.3.3 Probability color maps of the A-D test

As mentioned in section 4.3 the color maps only shows which distribution that performed best in the A-D test not how well the distribution performed. Another set of color maps was created but with the scale now instead showing how certain the A-D test have been for a specific distribution.

An example of such an image is figure 4.11, which shows how probable the test result has been for the Gamma distribution.

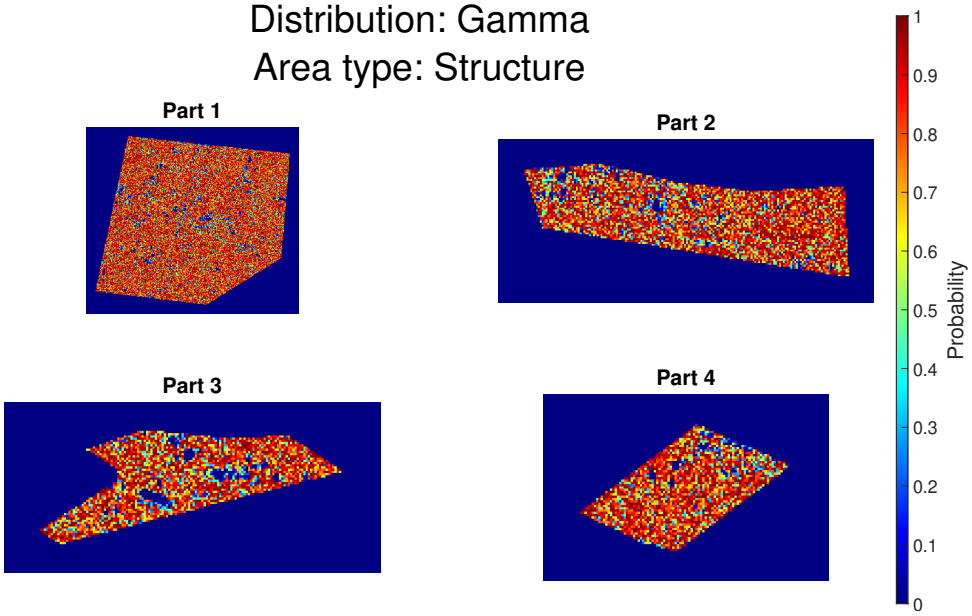

Figure 4.11: Probability plot for Gamma distribution.

A highly red color illustrates that the test result is very certain and a blue color show's a high uncertainty of the test. If the probability is lower than the significance level $\alpha = 0.05$ the A-D test would consider it a fail and reject the null hypotheses, which corresponds to a dark blue color in the probability images.

According to figure 4.11 it's been made clear that the Gamma distribution is highly probable for the structure area type. But what about those small clustered non-Gamma areas that have appeared where buildings are present. Taking a closer look at figure 4.9 both purple lognormal distribution clusters in Part 3 and red normal distribution clusters in Part 4 are visible. Comparing this information to the probability images of lognormal distribution, figure 4.12 and normal distribution, figure 4.13, it's possible to see that even though these two distributions had the best fit according to the A-D test, the probability that the lognormal and normal distribution is a good fit is much lower than that of the Gamma distribution for the rest of the pixels.

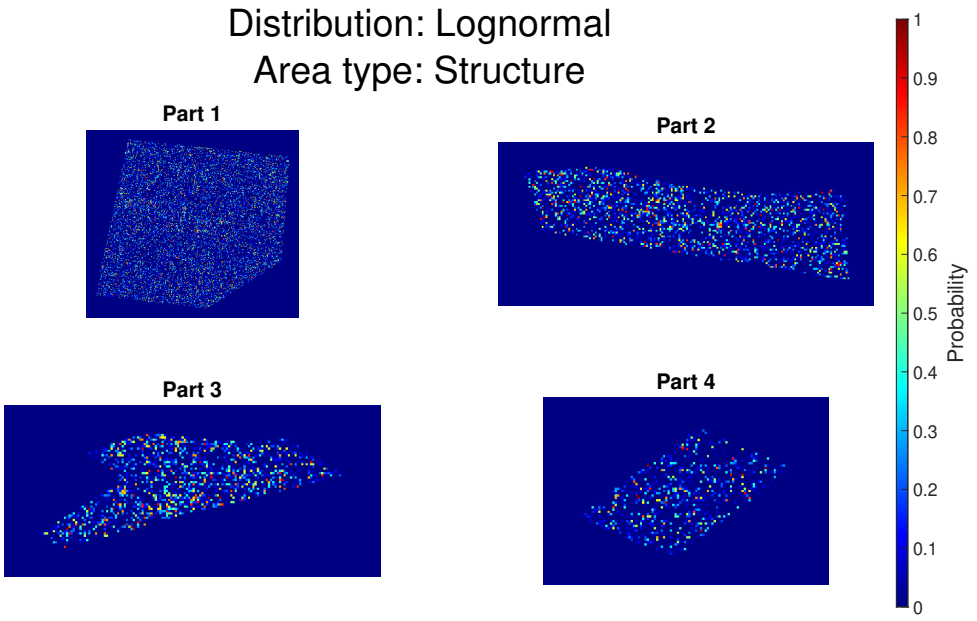

Figure 4.12: Probability plot for Lognormal distribution.

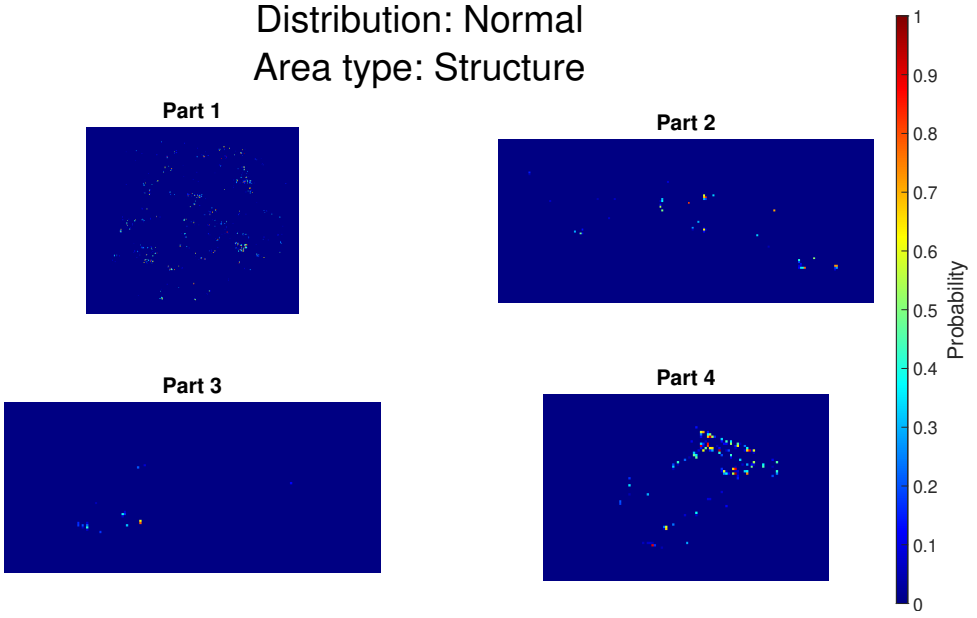

Figure 4.13: Probability plot for Normal distribution.

The most interesting color- and probability images have been included in this section. The color- and probability images for all target distribution models is included in Appendix B.

5
Conclusion & discussion

Two different image stacks of SAR intensity data containing different amounts of images have been investigated on how the temporal distribution of the data can be characterized. The SAR data have been tested against eight different target distribution models for a goodness-of-fit to see which of the target distribution models best fits to the data. The goodness-of-fit test have been made by the Anderson-Darling test.
The use of the A-D test together with looking for spatial patterns, e.g. in figure 4.9, allows for comparison of how well the different distribution models fit, even with the limited number of images available. From figure 3.2 it would appear impossible to decide which distribution fits, but the method gives clear objective results that the Gamma distribution model is a good fit.
The results have shown that the distribution of temporal SAR intensity data follows a Gamma distribution and is most likely to fit the data irrespective of the surface area types that have been investigated in this thesis. It's interesting to mention that if the same test would have been conducted with amplitude SAR data, instead of intensity, the rician and rayleigh distribution models would probably perform better. The reason would be because the distribution for pure speckle follows a Rayleigh distribution for amplitude data but the speckle follows an exponential distribution model for intensity data. And the Gamma distribution is a special case of the Exponential distribution, with shape parameter = 1, which could be a reason why the Gamma distribution performs well for intensity data. The color images in section 4.3.2 interestingly shows that none of the target distributions that have been investigated throughout this thesis seem to make a good fit over actual structures and buildings. The reason for this could be that the number of images in the image stacks are too few. This could be validated by the clear difference in the percentage of how often the Gamma distribution fits between the first and second image stack, which had 26 and 64 images respectively. Since more than twice the amount of images are present in the second image stack you could assume a noticeable increase in how well the Gamma distribution should have performed, which was the case shown in tables 4.1 and 4.2. In general the K-distribution would have been an interesting candidate to take a closer look at since it has previously been proven to be a good fit for SAR data in a spatial scenario. The K-distribution could possibly be a strong candidate distribution for the buildings since no other distribution seem to make a good fit to that type of data.

6
Future Work

There are a few things that would be interesting to investigate further on.

- **Adding more distributions**
  To add more distributions to the target distribution table listen in table 2.2 could prove valuable to see if there are any other distributions that would fit the data. Especially to find a distribution that would better fit the data for the buildings within a structure area type. Possibly could the K-distribution be an interesting distribution to implement.
- **Larger image stacks**
  To perform a similar investigation on a larger image stack to see if the result can be improved. The parameter approximation should improve and thus also the ability to match the data to a correct statistical distribution.
- **Change detection**
  To continue this work and implement a change detection algorithm to be able within one or just a few pixel positions detect if a change has occurred by adding a new image to the image stack. One usefulness of this thesis work is that the detection algorithm can be chosen to be different for different pixels depending on which distribution best fits the data.
- **Ice on lakes**
  The case shown in figure 4.6 where a few SAR images containing ice patches was enough to make the Gamma distribution model perform worse than the Lognormal distribution model. It would be interesting to further investigate how few images are needed, with ice present, to change the conclusion which distribution model has the best fit.
- **Use different types of SAR images**
  It would be interesting to extend this kind of analysis to a larger variety of geographically different areas, where seasonal changes might be different. Also to use different kinds of SAR data, e.g. higher resolution images and different frequency bands.
- **Investigate how dependent samples affect the A-D test**
  The A-D test assumes independent samples. The data used in this thesis has not been completely independent thus would it be interesting to further investigate, for example by simulations, how partially dependent samples affect the results of the A-D test.

Bibliography

[1] Google maps. [Online]. Available: https://goo.gl/maps/GbccRjWLC3i9KzBRA

[2] C. Oliver and S. Quegan, *Understanding Synthetic Aperature Radar Images*. 685 Canton Street, Norwood, MA 02062: Artech House, Inc, 1998.

[3] A. Moreira, P. Prats-Iraola, M. Younis, G. Krieger, I. Hajnsek, and K. P. Papathanassiou, "A tutorial on synthetic aperture radar," *IEEE Geoscience and Remote Sensing Magazine*, vol. 1, no. 1, pp. 6–43, 2013.

[4] What is SAR? [Online]. Available: https://asf.alaska.edu/information/sar-information/what-is-sar/

[5] M. Soja, "Modelling and Retrieval of Forest Parameters from Synthetic Aperture Radar Data," Ph.D. dissertation, Chalmers University of Technology, Department of Earth and Space Sciences, Sweden, 2014, http://publications.lib.chalmers.se/records/fulltext/208148/208148.pdf.

[6] F. Argenti, A. Lapini, T. Bianchi, and L. Alparone, "A Tutorial on Speckle Reduction in Synthetic Aperture Radar Images," *IEEE Geoscience and Remote Sensing Magazine*, vol. 1, no. 3, pp. 6–35, 2013.

[7] G. Krieger, A. Moreira, H. Fiedler, I. Hajnsek, M. Werner, M. Younis, and M. Zink, "TanDEM-X: A Satellite Formation for High-Resolution SAR Interferometry," *IEEE Transactions on Geoscience and Remote Sensing*, vol. 45, no. 11, pp. 3317–3341, 2007.

[8] M. J. Soja, J. I. H. Askne, and L. M. H. Ulander, "Estimation of Boreal Forest Properties From TanDEM-X Data Using Inversion of the Interferometric Water Cloud Model," *IEEE Geoscience and Remote Sensing Letters*, vol. 14, no. 7, pp. 997–1001, 2017.

[9] NIST/SEMATECH. (2013) NIST/SEMATECH e-Handbook of Statistical Methods. [Online]. Available: https://www.itl.nist.gov/div898/handbook/eda/section3/eda35g.htm

[10] I. R. Joughin, D. B. Percival, and D. P. Winebrenner, "Maximum likelihood estimation of K distribution parameters for SAR data," *IEEE Transactions on Geoscience and Remote Sensing*, vol. 31, no. 5, pp. 989–999, 1993.

[11] T. W. Anderson and D. A. Darling, *Ann. Math. Statist.*

[12] D. I. Alves, B. G. Palm, M. I. Pettersson, V. T. Vu, R. Machado, B. F. Uchôa-Filho, P. Dammert, and H. Hellsten, "A Statistical Analysis for Wavelength-Resolution SAR Image Stacks," *IEEE Geoscience and Remote Sensing Letters*, vol. 17, no. 2, pp. 227–231, 2020.

[13] Anderson-Darling statistic. [Online]. Available: https://encyclopediaofmath.org/wiki/Anderson-Darling_statistic

[14] R. B. D'Agostino and M. A. Stephens, *Goodness-of-Fit Techniques*. USA: Marcel Dekker, Inc., 1986.

[15] J. Marsaglia and G. Marsaglia, "Evaluating the Anderson-Darling Distribution," *Journal of Statistical Software*, vol. 09, 02 2004.

[16] Probability concepts explained: Maximum likelihood estimation. [Online]. Available: https://towardsdatascience.com/probability-concepts-explained-maximum-likelihood-estimation-c7b4342fdbb1

[17] What is the difference between Method Of Moment (MOM), Maximum A Posteriori (MAP), and Maximum Likelihood Estimation (MLE)? [Online]. Available: https://www.quora.com/What-is-the-difference-between-Method-Of-Moment-MOM-Maximum-A-Posteriori-MAP-and-Maximum-Likelihood-Estimation-MLE

[18] J. V. Psutka and J. Psutka, "Sample Size for Maximum Likelihood Estimates of Gaussian Model," in *Computer Analysis of Images and Patterns*, G. Azzopardi and N. Petkov, Eds. Cham: Springer International Publishing, 2015, pp. 462–469.

[19] I. The MathWorks. (2020) MATLAB webpage. [Online]. Available: https://www.mathworks.com/products/matlab.html

[20] G. LLC. (2020) Google Maps Webpage. [Online]. Available: https://www.google.se/maps

[21] Anderson-Darling Test for Normality. [Online]. Available: https://www.spcforexcel.com/knowledge/basic-statistics/anderson-darling-test-for-normality

[22] E. E. Online. (2020) Parameters affecting radar backscatter. [Online]. Available: https://earth.esa.int/web/guest/missions/esa-operational-eo-missions/ers/instruments/sar/applications/radar-courses/content-2/-/asset_publisher/qIBc6NYRXfnG/content/radar-course-2-parameters-affecting-radar-backscatter

[23] G. Schwaizer. (2017) SAR / Optical Applications to Ice and Snow. [Online]. Available: https://earth.esa.int/documents/10174/3166008/ESA_Training_Vilnius_07072017_SAR_Optical_Snow_Ice_Lecture_Schwaizer.pdf

[24] SMHI. (2020) LUFTTEMPERATUR (H). [Online]. Available: https://www.smhi.se/data/meteorologi/ladda-ner-meteorologiska-observationer/#param=airtemperatureInstant,stations=all,stationid=149120

A

Appendix A - Detailed SAR Image file information

Table A.1: Table showing filenames for all images in both image stacks. The image timestamps for image stack 1 is 16:12 and for image stack 2 is 05:05 UTC.

Image Stack 1	**Image Stack 2**	
Filename	**Filename**	
20110617_TSX	20130430_TSX	20131103_TSX
20110617_TDX	20130430_TDX	20131103_TDX
20110720_TSX	20130511_TSX	20131114_TSX
20110720_TDX	20130511_TDX	20131114_TDX
20110811_TSX	20130522_TSX	20131206_TSX
20110811_TDX	20130522_TDX	20131206_TDX
20110822_TSX	20130602_TSX	20131228_TSX
20110822_TDX	20130602_TDX	20131228_TDX
20120225_TSX	20130613_TSX	20140119_TSX
20120225_TDX	20130613_TDX	20140119_TDX
20120717_TSX	20130624_TSX	20140210_TSX
20120717_TDX	20130624_TDX	20140210_TDX
20120808_TSX	20130705_TSX	20140428_TSX
20120808_TDX	20130705_TDX	20140428_TDX
20120819_TSX	20130716_TSX	20140520_TSX
20120819_TDX	20130716_TDX	20140520_TDX
20130601_TSX	20130727_TSX	20140531_TSX
20130601_TDX	20130727_TDX	20140531_TDX
20130623_TSX	20130818_TSX	20140622_TSX
20130623_TDX	20130818_TDX	20140622_TDX
20130726_TSX	20130829_TSX	20140703_TSX
20130726_TDX	20130829_TDX	20140703_TDX
20131227_TSX	20130909_TSX	20140714_TSX
20131227_TDX	20130909_TDX	20140714_TDX
20140713_TSX	20130920_TSX	20140725_TSX
20140713_TDX	20130920_TDX	20140725_TDX
20140826_TSX	20131001_TSX	20140816_TSX
20140826_TDX	20131001_TDX	20140816_TDX
	20131012_TSX	20140827_TSX
	20131012_TDX	20140827_TDX
	20131023_TSX	20140907_TSX
	20131023_TDX	20140907_TDX

B

Appendix B - Color maps

B.1 Image Stack 1

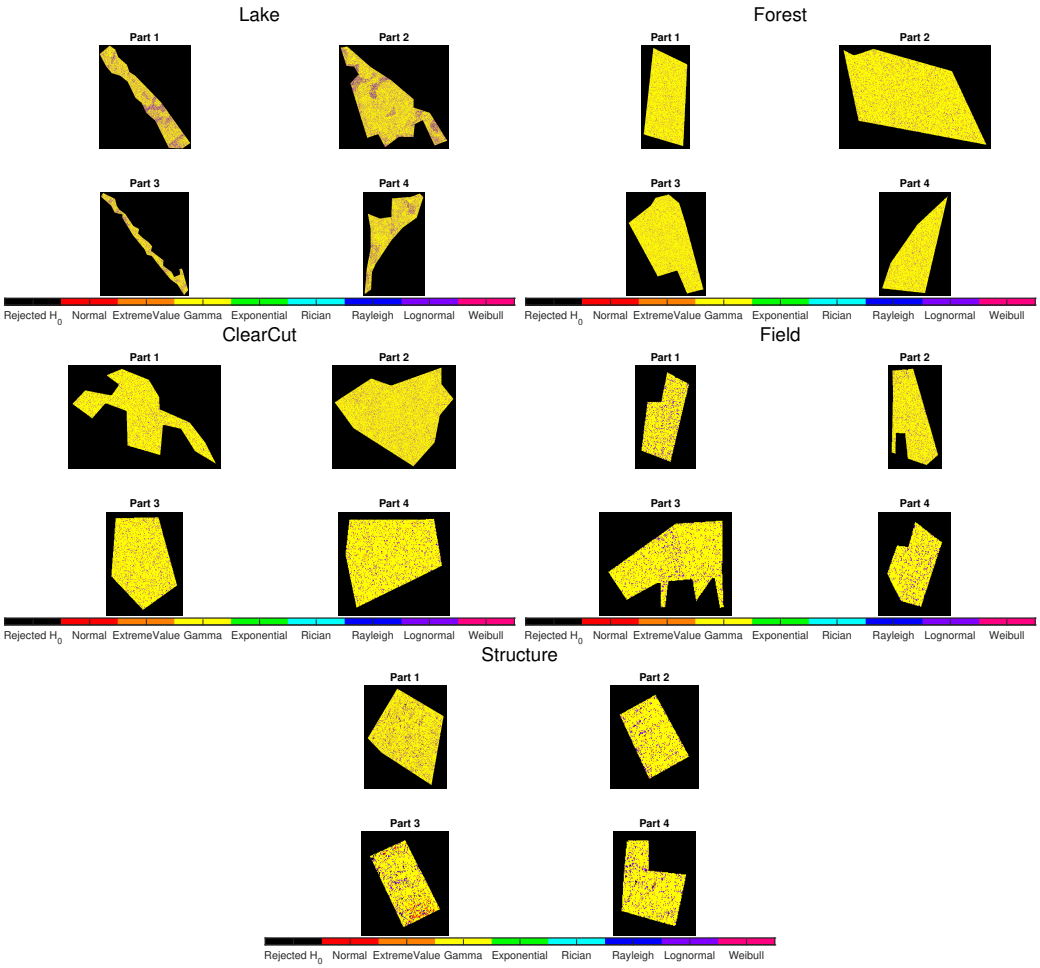

Figure B.1: Color map of which distribution had the best fit to data for all area types.

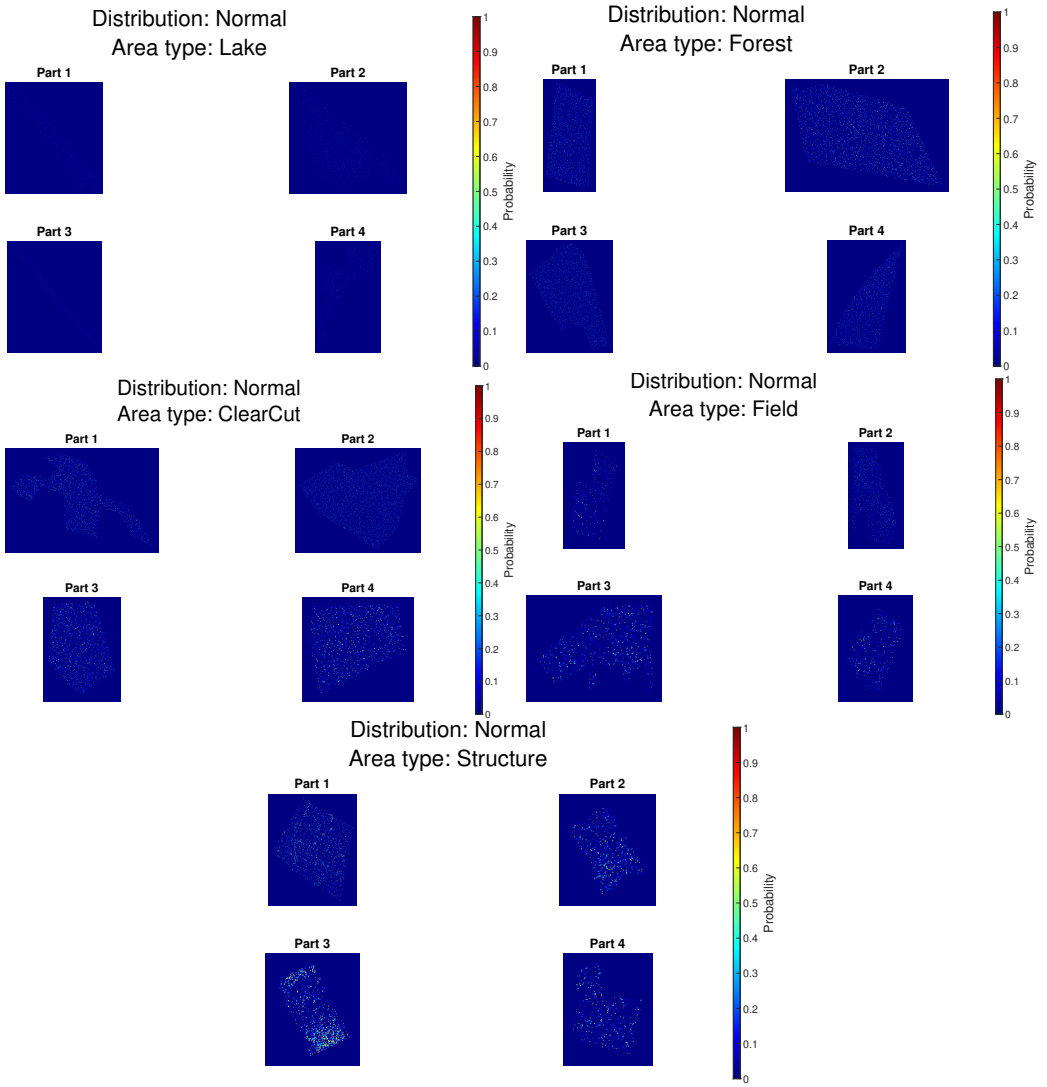

Figure B.2: Probability plots for Normal distribution for all area types.

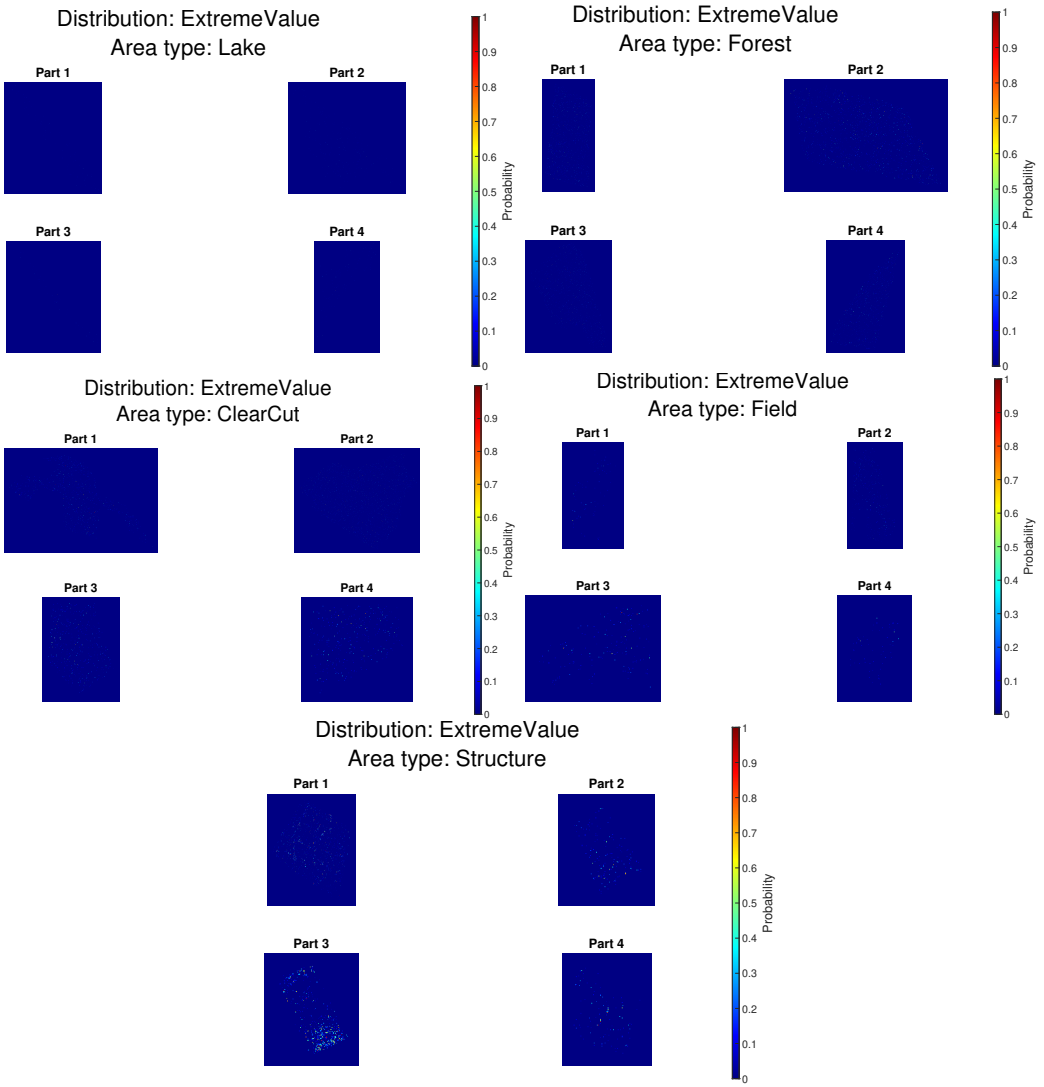

Figure B.3: Probability plots for Extreme Value distribution for all area types.

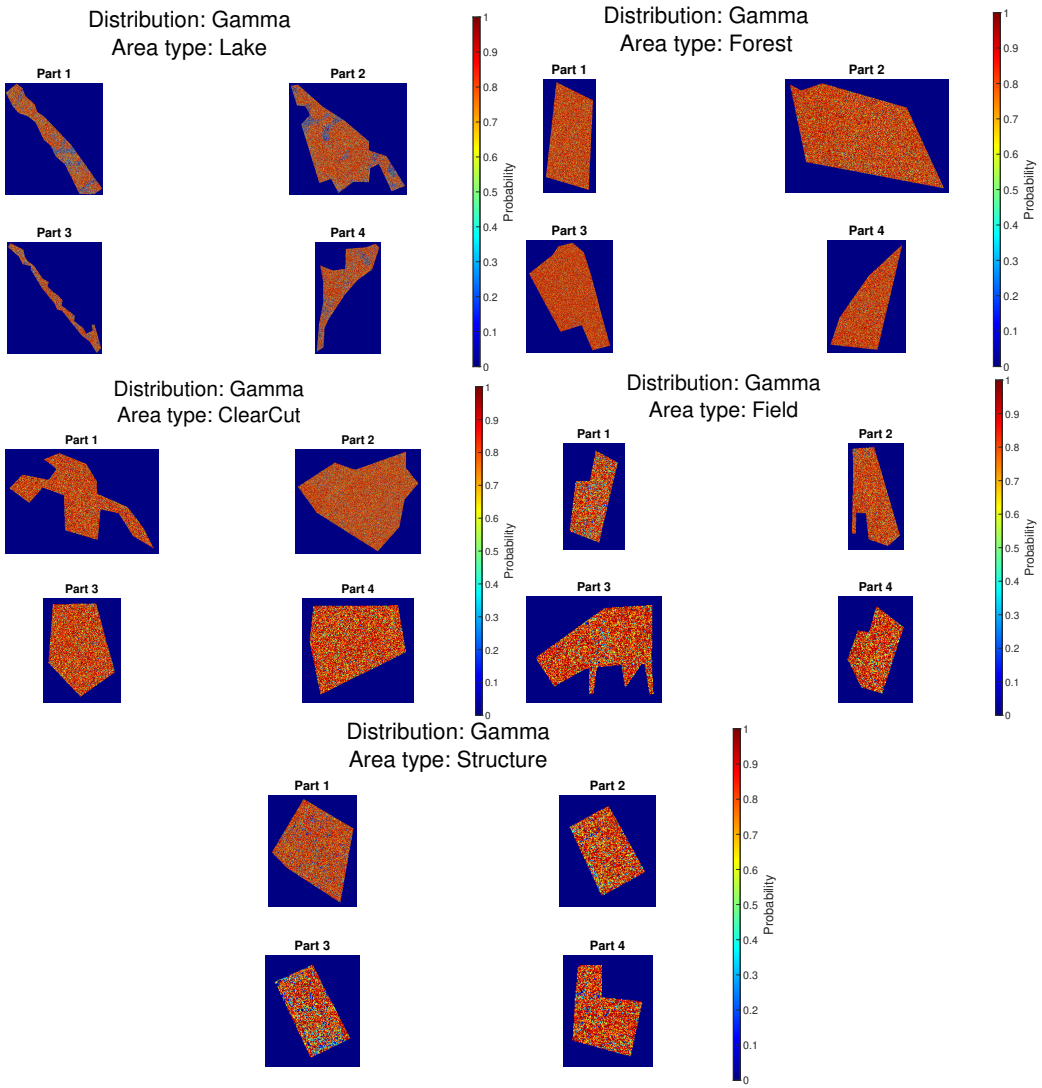

Figure B.4: Probability plots for Gamma distribution for all area types.

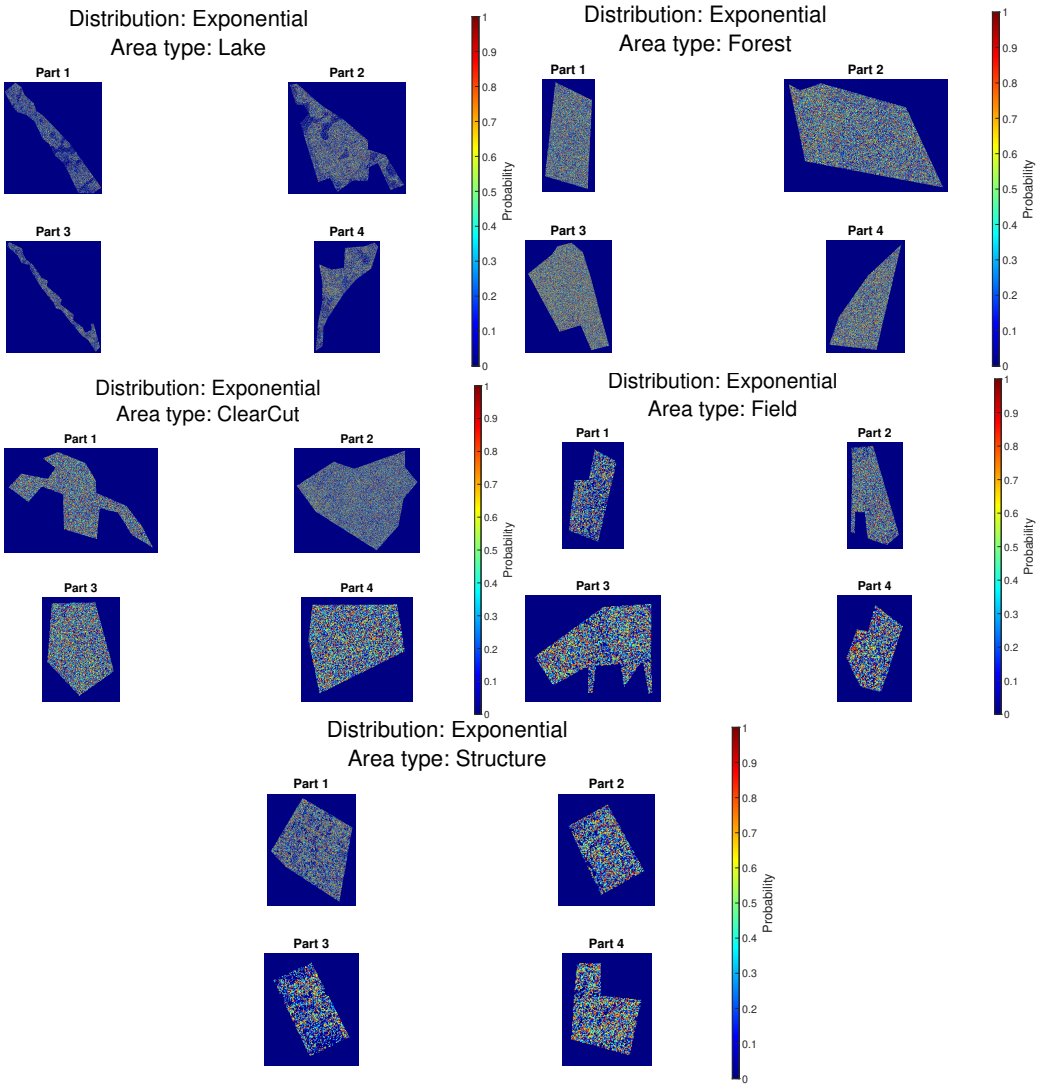

Figure B.5: Probability plots for Exponential distribution for all area types.

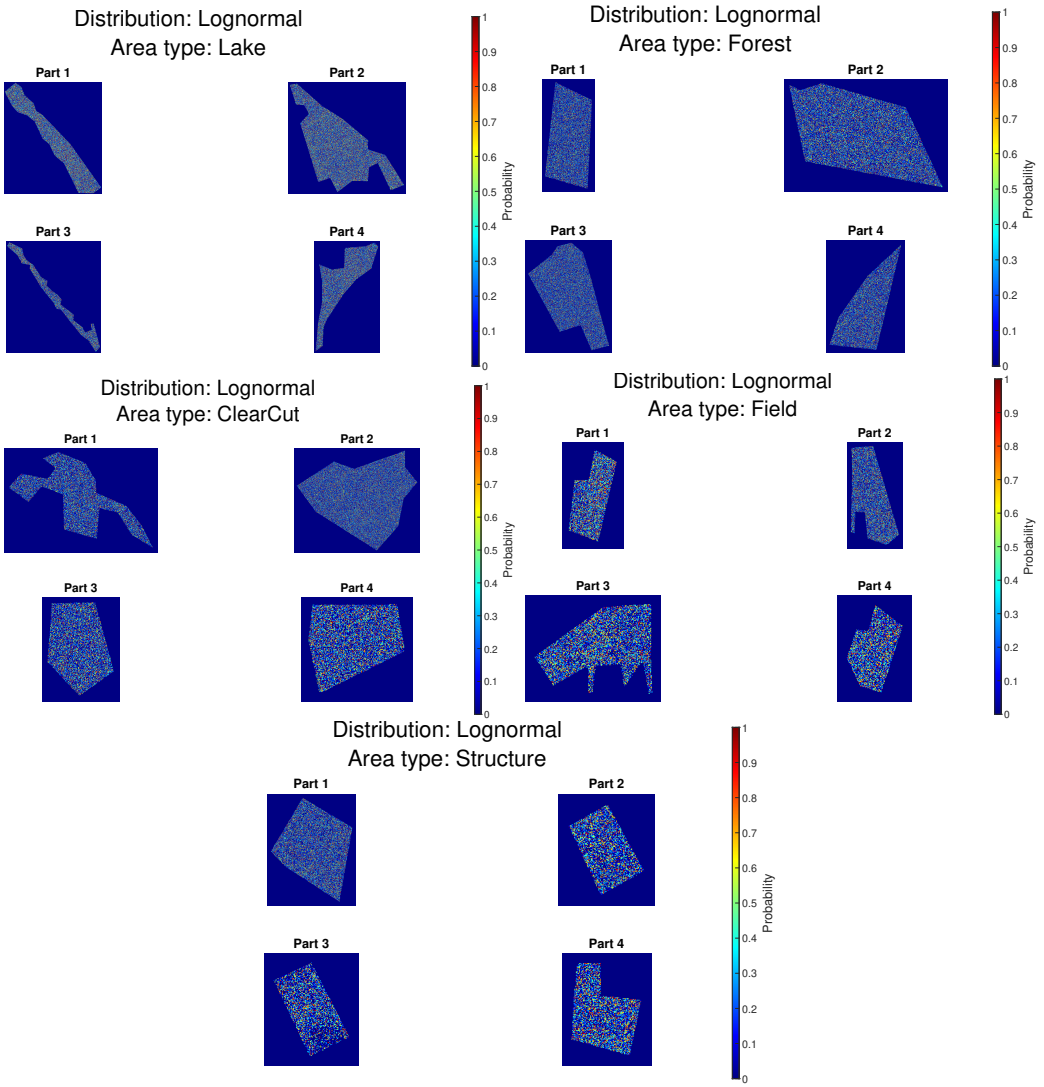

Figure B.6: Probability plots for Lognormal distribution for all area types.

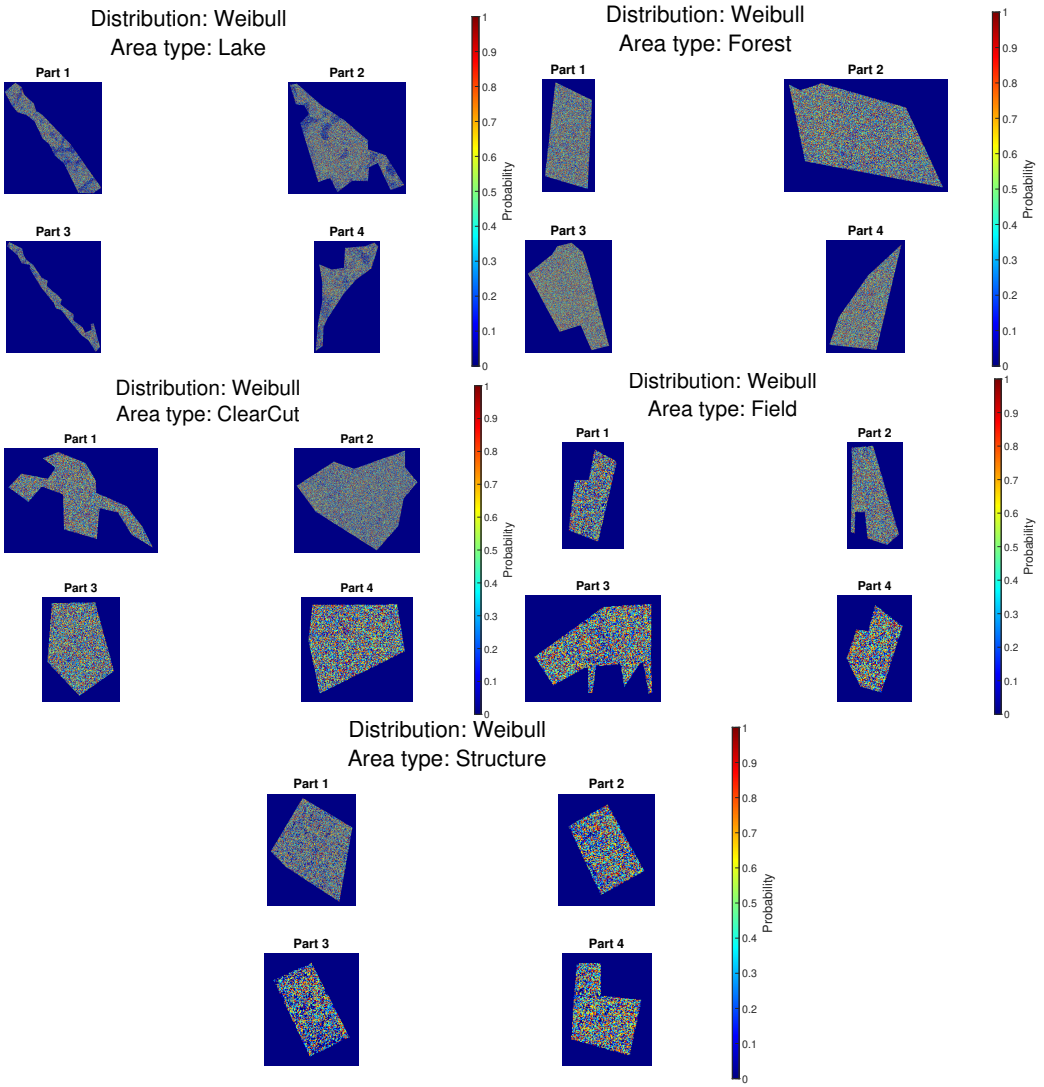

Figure B.7: Probability plots for Weibull distribution for all area types.

B.2 Image Stack 2

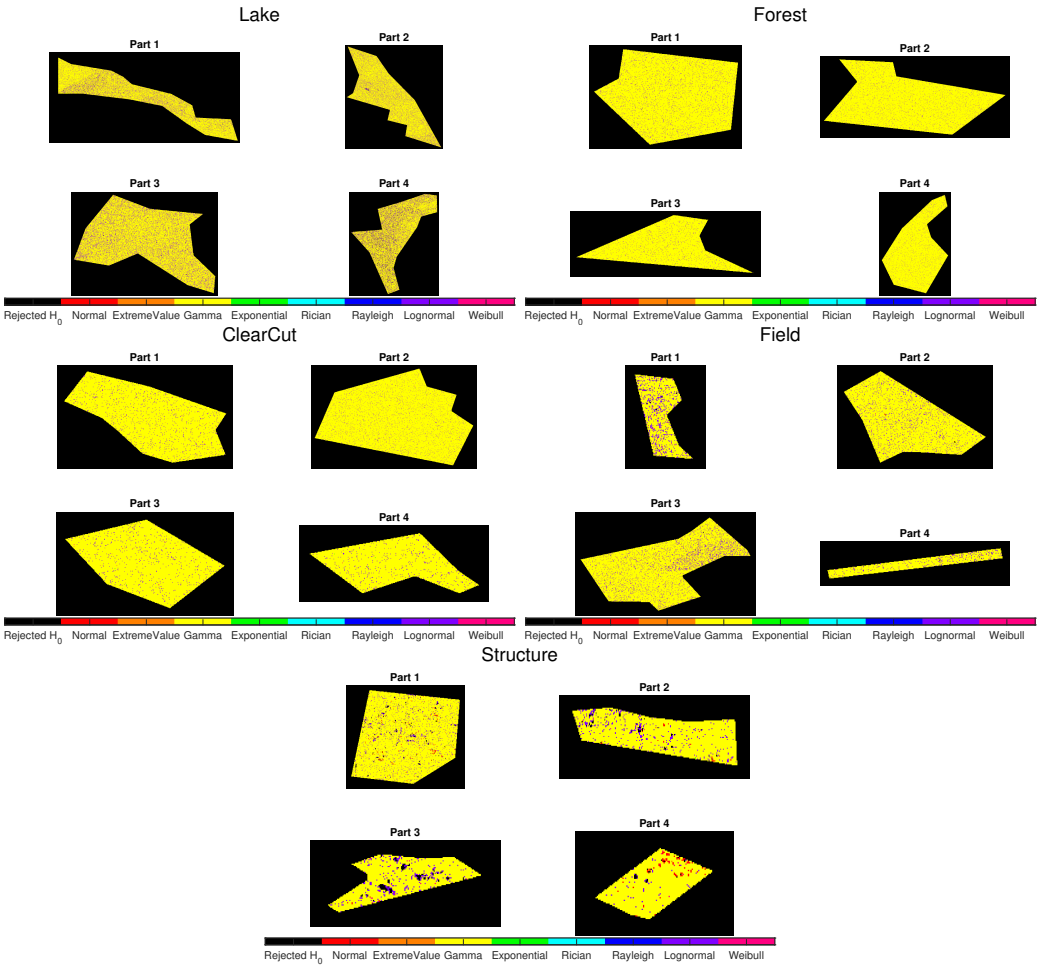

Figure B.8: Color map of which distribution had the best fit to data for all area types.

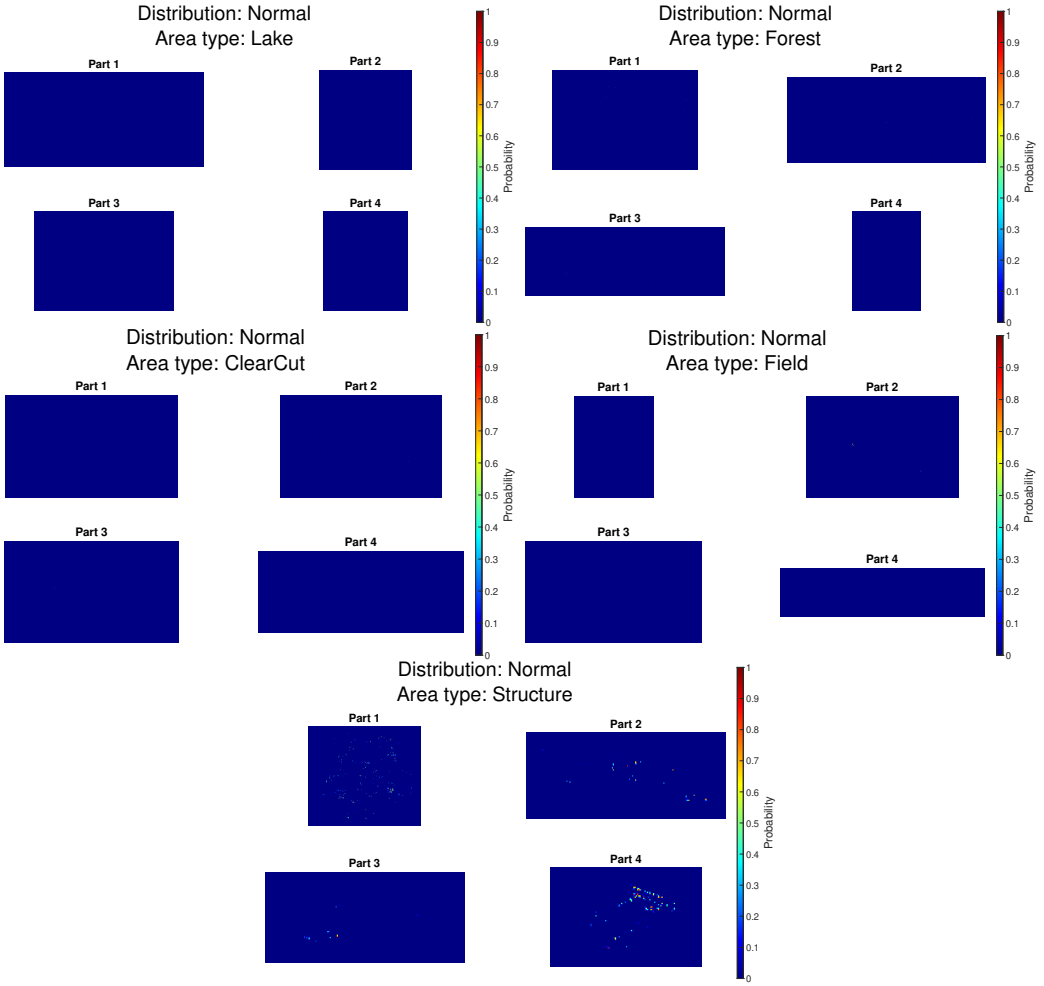

Figure B.9: Probability plots for Normal distribution for all area types.

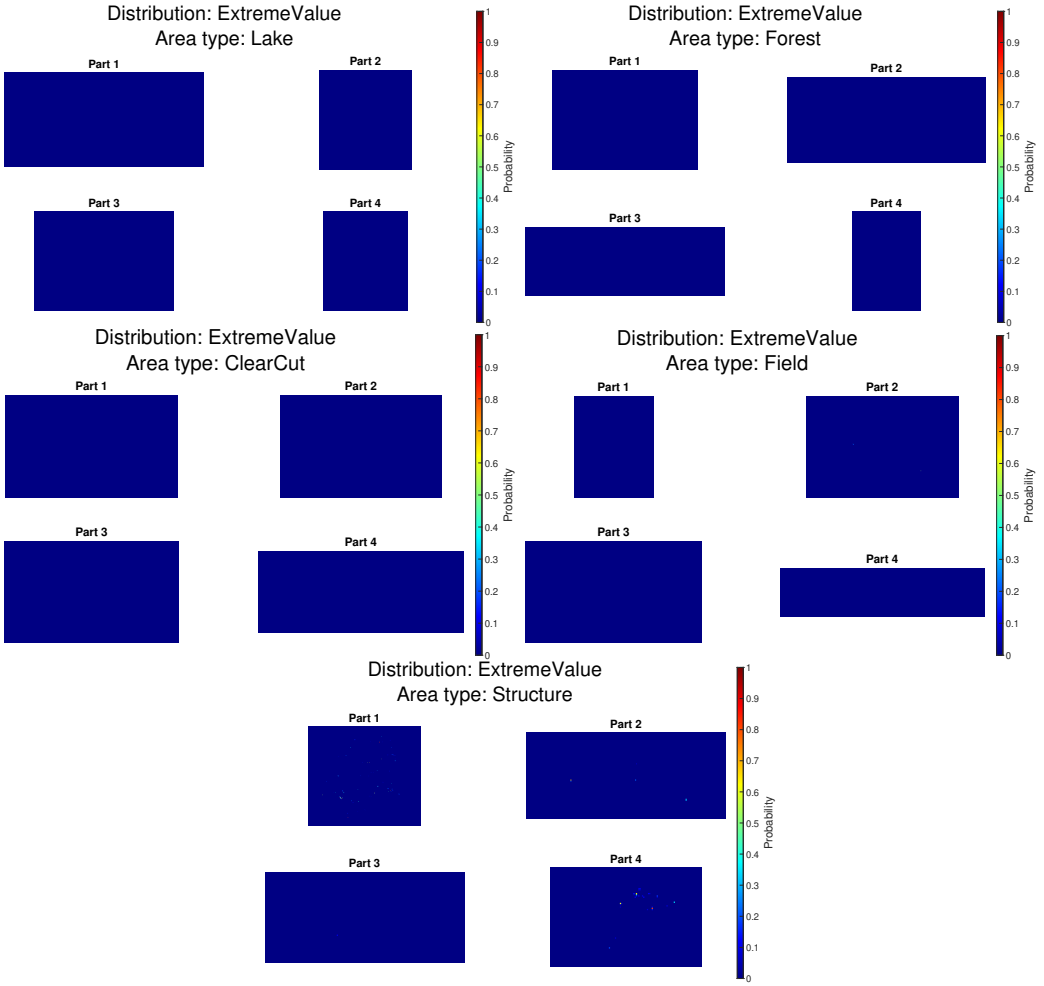

Figure B.10: Probability plots for Extreme Value distribution for all area types.

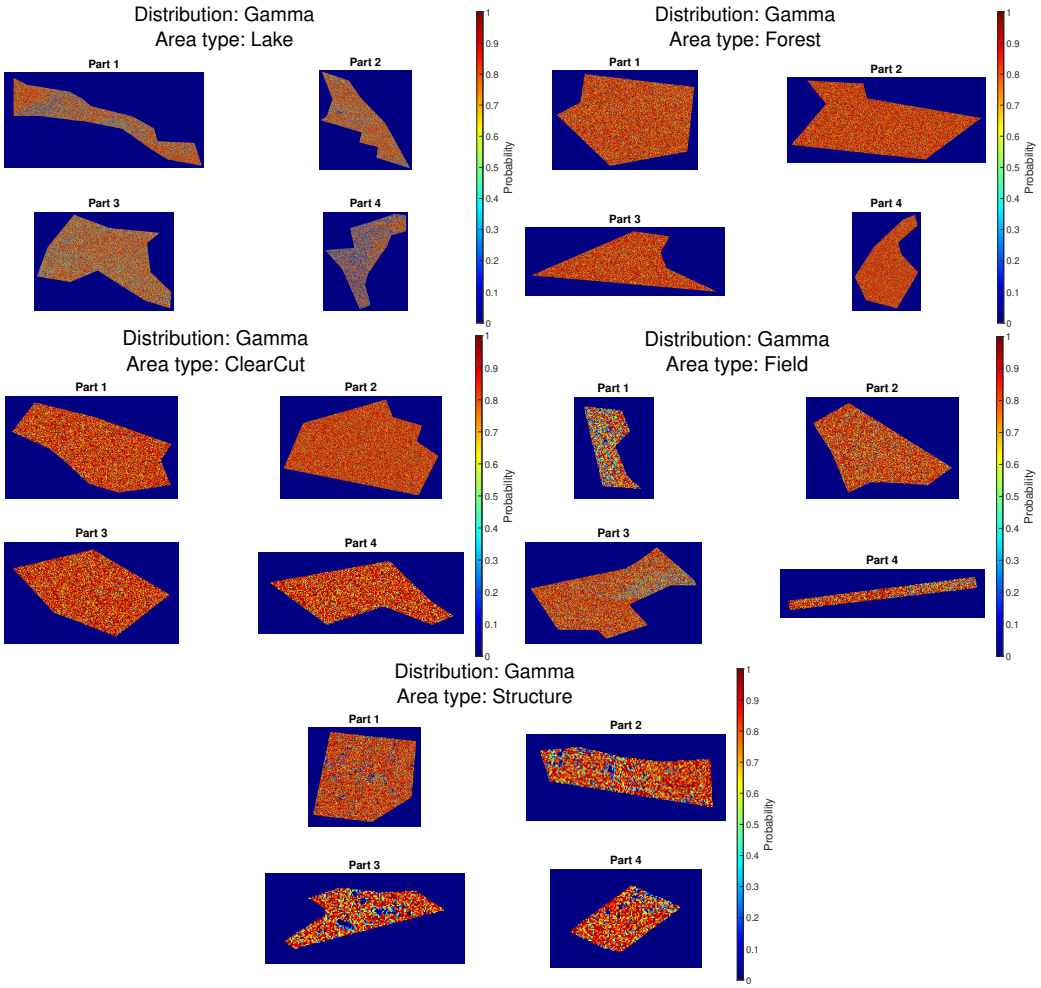

Figure B.11: Probability plots for Gamma distribution for all area types.

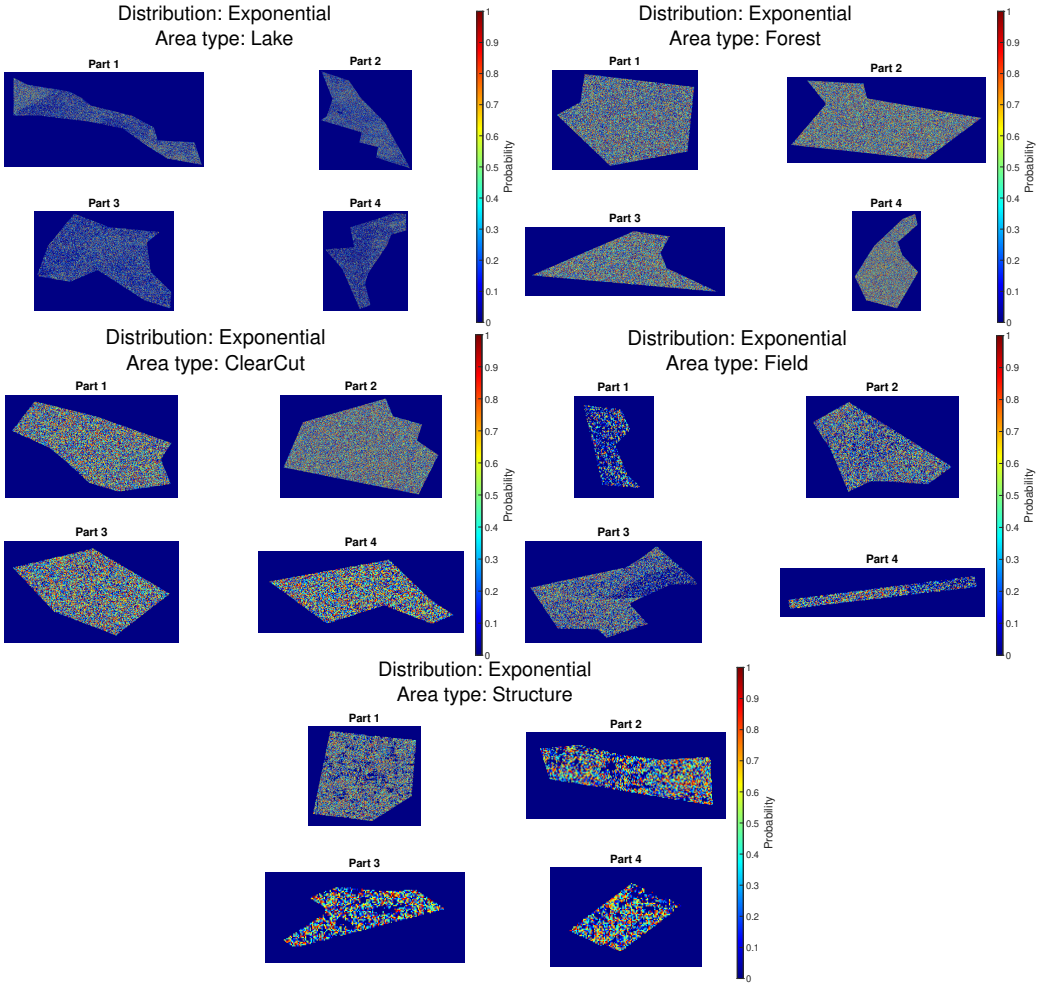

Figure B.12: Probability plots for Exponential distribution for all area types.

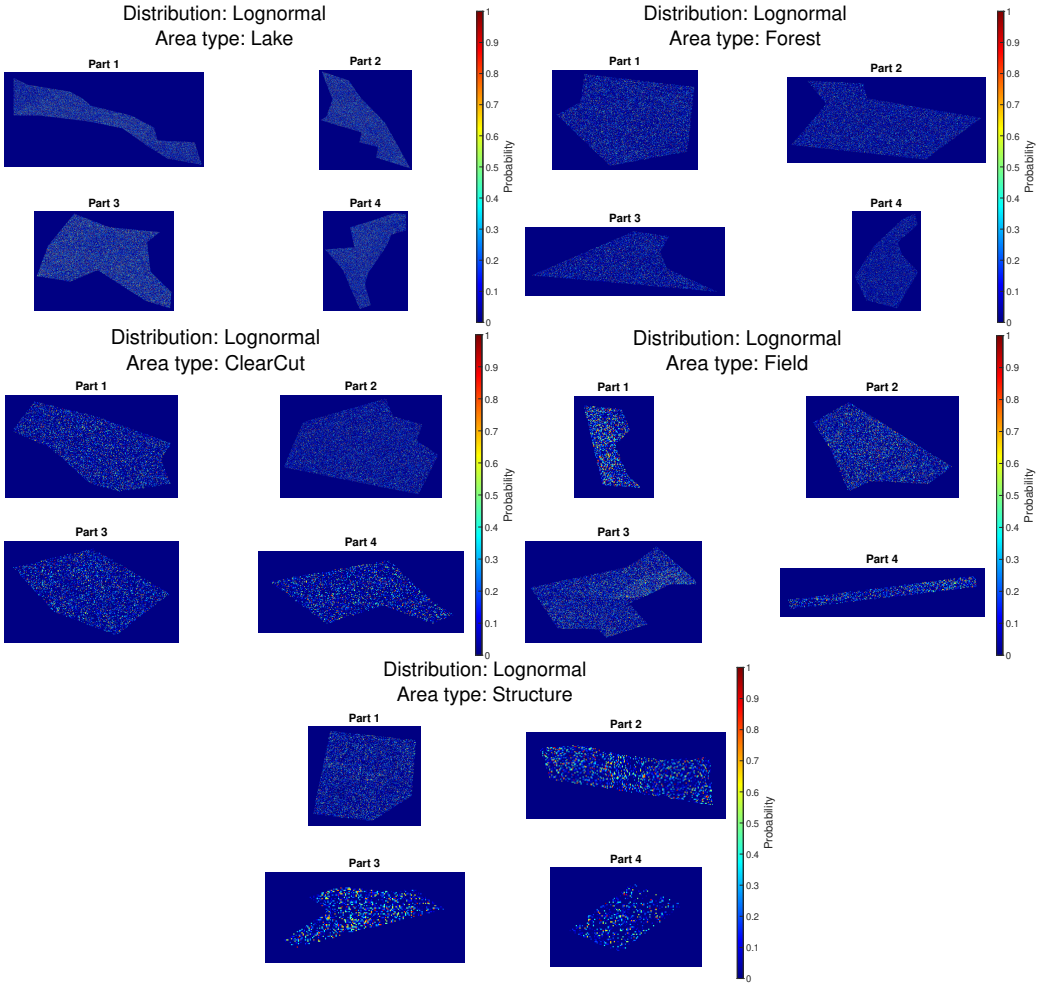

Figure B.13: Probability plots for Lognormal distribution for all area types.

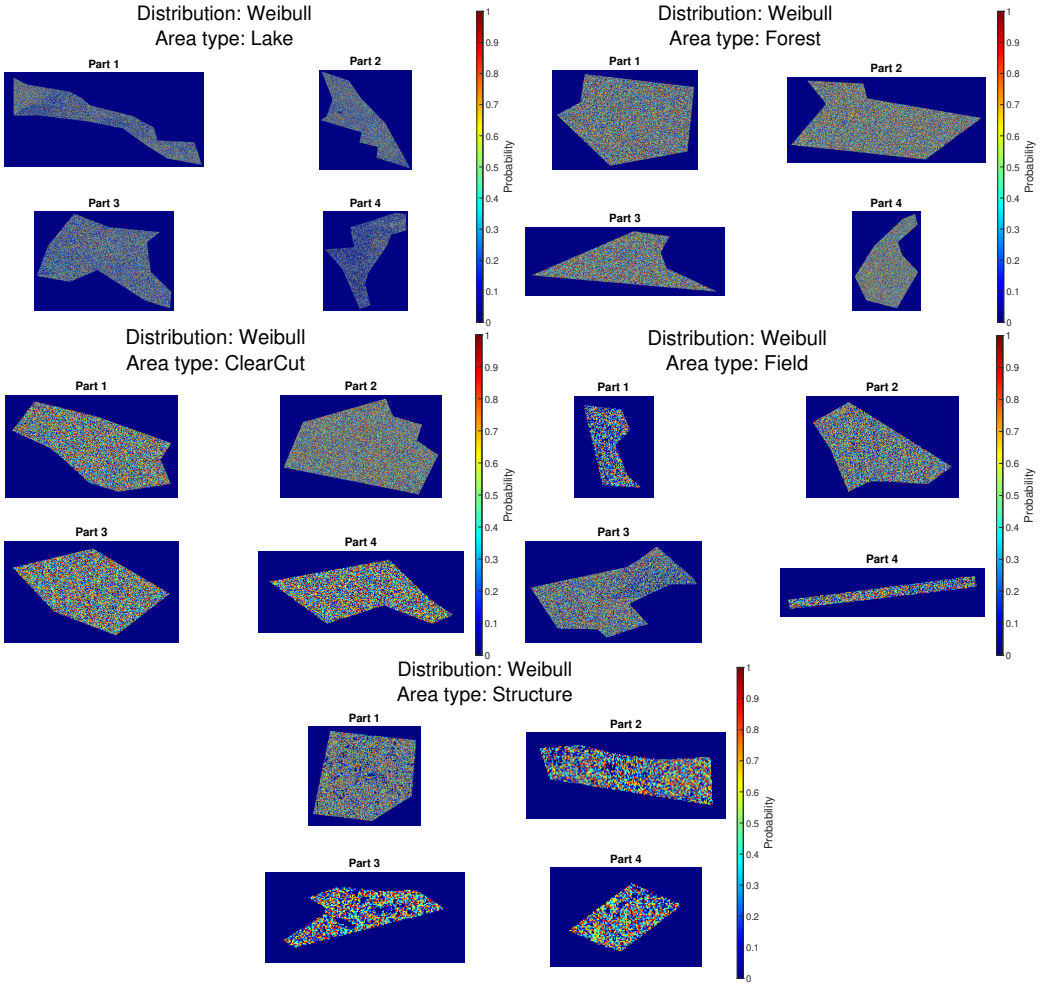

Figure B.14: Probability plots for Weibull distribution for all area types.